MARSTER'S THESIS

A STUDY OF THE β^- RESPONSE OF SILICON DETECTORS AND THE EFFECTS OF BACKSCATTERING IN A COMPLEX SETUP USING GEANT4

Sheila Lærkegaard Johansen
201606295

Supervisor: Karsten Riisager

Department of Physics and Astronomy
Aarhus University
June 14, 2021

AARHUS
UNIVERSITY

Abstract

A study of the β^- response of two different kinds of silicon detectors and the effects backscattering can have on the β^- response is presented. This was achieved using the Monte Carlo framework, Geant4, which specializes in simulating particles traversing matter. The study has been applied to the complex experimental setup used for experiments at IGISOL by the Aarhus University Subatomic Physics Group in 2020. Mainly two different analysis have been provided; an analysis with a monoenergetic β^- source, and an analysis with a realistic ^{12}B source both with an without a realistic threshold. Furthermore, an analysis of the setup using an α particle source yielded a solid angle coverage of 54.32(2)%. The analysis using the realistic ^{12}B source showed that the combination of the detectors, the detector frames, and the 3D printed cube resulted in 7.86(6)% more particles being detected compared to the ideal case where no particles are backscattered and the main contributor was the detectors. Analyzing the angular distribution of the β particles, we saw that the combination of the detectors, their frames, and the cube changed the angular distribution in the setup considerably. Adding a threshold of 250 keV also changed the angular distribution of the β particles. Additionally, we also saw that the effect of backscattering was largest for sources with lower energies - in particular we saw that the effect of backscattering for ^{6}He resulted in 19.12(7)% more particles being detected compared to the ideal case where no particles are backscattered. Concluding, this means that in general backscattering must be taken into account when doing experiments with β^- particles. Furthermore, new simulations must be made when either the setup, the source, or the detectors are changed, as this can have an effect on the characteristics of the backscattering in the setup.

Acknowledgements

At first, I would like to thank my supervisor, Karsten Riisager, for his always competent supervision and his positive mindset. He has spent numerous hours discussing and guiding me through the process of writing this thesis.

I would also like to express my gratitude to Erik Jensen and especially Andreas Gad, who have patiently helped with all the technical aspects of this project including several hours of installing and debugging. Without the help of Andreas, this project would not have been possible.

Furthermore, I would like to thank my study partner, Lasse Falck Nissen, for his support and company which has made a big difference while writing a thesis under a lockdown in a pandemic.

Lastly, I would like to thank my boyfriend, Asger Drewsen, for his support and technical help and my family especially my sister, Sandie Johansen, for their love and support.

Sheila Lærkegaard Johansen

Aarhus, June 2021

Table of contents

Introduction

The main objective of this thesis has been to study the β response of two different kinds of silicon detectors and to study the effects of backscattering of β particles in a complex experimental setup using the Monte Carlo framework, Geant4.

The main motivation of this study should be found in the first analysis of the $\beta\alpha$ correlations of the β^- decay of ^{12}N performed by a former PhD student, R. Gark from York. This first analysis showed unexpected angular correlations for the decay of ^{12}N [3] and thus it has been of interest to study the mirror decay to see if these angular correlations also occur here. To be able to study the mirror decay, experiments with ^{12}B has been performed by the Aarhus University Subatomic Physics Group at IGISOL in 2020.

Before a further analysis of the data of the two mirror decays is performed, it is of interest to study the effects of backscattering in the setup, as the effects this can have on the angular distributions of β^- particles was to our knowledge still unknown before the work presented in this thesis.

It is, though, well known that β particles are backscattered in a setup. But before the work presented in this thesis, we did not know how large the effect is and if backscattering can change the angular distribution of the β^- particles. Thus, it was of interest to study these effects of backscattering to see if they can be part of the explanation to the surprising angular correlations.

The two experiments with the mirror decays have been performed using different setups. The experiment performed at IGISOL with ^{12}B used a more advanced setup with a 3D printed cube compared to the experiments with ^{12}N. As this cube might cause the effect of backscattering in the setup to increase, we have chosen to focus on simulating the setup used at IGISOL together with the ^{12}B source.

To study the effects of backscattering in the complex setup used by the Aarhus University Subatomic Physics group at IGISOL, Monte Carlo simulations was used. Apart from Monte Carlo simulations, a more theoretical approach could also have been chosen but when a problem has so many degrees of freedom,

Monte Carlo Simulations are a great tool for solving the problem. The choice of using Monte Carlo simulations also gives us the freedom to easily change things if the program should be used for studying other setups, detectors, sources etc.

The detectors used at IGISOL have been simulated by S. Viñals [14] and thus these simulations have been used for inspiration. In this thesis, the same design has been used for simulating the detectors but the simulations have been build upon G4Sim as described in section 2.2. This means that inspiration has been drawn from the work of S. Viñals but the code itself has been produced from the starting point of G4Sim as part of this thesis. Furthermore, S. Viñals only implemented the detector and thus the work regarding the implementation of the other parts of the setup have been build from scratch.

The focus of this thesis has thus been to produce a program enabling us to study the effects of backscattering in the setup and furthermore to gain an insight into the order of magnitudes of the effects of backscattering in the setup. As a result of this, visual analysis has mainly been chosen as this will help us get an understanding of the characteristics and importance of the effects of backscattering.

Chapter 1

Facts and concepts

As the name of the chapter hints, this chapter both contains background knowledge but also some facts and information on the simulated experiment. This means that some of the sections in the chapter do not follow a common thread - but the information will be of importance later on.

The chapter has four main parts. section 1.1 describes how particles interact with matter and how this relates to the detectors studies in this thesis.section 1.2 describes the realistic source which has mainly been used in this thesis, and section 1.3 describes the types of detectors which has been used and how these work. section 1.4 differs from the previous parts as this contains the most critical information on the experiment which has been simulated in this thesis. The information described in the first three parts of this chapter can be found in the book "Radiation detection and measurements" by F. Knoll Glenn, [6]. The book contains a far more detailed description of the concepts but the main structure of the book has been followed in this chapter.

You should also note, that in the rest of this thesis, β particles will be mentioned quite a lot. As this thesis is only concerned with β^- decay and hence β^- particles, this means that when β particles are mentioned onward, it is implicit that we actually mean β^- particles and hence electrons.

1.1 Particles interacting with matter

When particles interact with matter the interactions depend on several factors including the type of particle and the material of the matter. In this thesis, we will mainly be concerned with electrons interacting with silicon detectors but we will also look at α particles interacting with the detectors. These two kinds of particles interact with matter in different ways and in the following sections we go through how heavy particles such as α particles and how fast electrons, β^- particles, interact with matter.

1.1.1 Heavy charged particles (α particles)

Heavy charged particles, such as α particles, can interact with atoms in detector materials in two ways; they can either interact with the orbital electrons or with the nuclei of the atoms. In general, it is very rare that alpha particles interact with the nuclei of the atoms and thus the effect of this interaction will not be prominent. The main reason for the energy loss of α particles is hense the interactions with the orbital electrons of the detector materials.

This effect is a result of the α particles interacting with the orbital electrons of the detector materials through the Coulomb force. More specifically, the positive charge of the α particles will interact with the negative charge of the orbital electrons of the atoms in the detector which will lead to energy transmission.

When an α particle traverses the detector, it will interact with many of the orbital electrons simultaneously. For each interaction, the electron will either be excited or completely removed from its atom depending on the amount of transferred energy. This energy comes from the α particle, and therefore, the interaction results in the α particle decreasing its energy and hence its velocity with each interaction. In one interaction, a heavy particle can only transfer around 1/500 of its energy per nucleon to the electron. As this is a relatively small amount of energy, the particles will slowly but consistently lose energy and hence slow down steadily when interacting with many such orbital electrons.

This process of energy loss results in heavy particles traversing the detector in a nearly linear path. The linear path is caused by the fact that the heavy particle interacts with many electrons in different directions simultaneously and as any single electron will not deflect the heavy particle significantly, the sum of all of the simultaneous encounters will result in a nearly linear path.

As a result, heavy charged particles will have a specific range in a given material which is described by the linear stopping power,

$$S = -\frac{dE}{dx}, \tag{1.1}$$

where $\frac{dE}{dx}$ is the particles rate of energy loss.

The stopping power of a heavy particle is not constant as it varies inversely with the energy of the traversing particle namely as $1/v^2$. This makes sense in the way, that if a particle has a lower velocity, it will spend a larger amount of time in the vicinity of a given orbital electron resulting in a larger energy transfer. If the particle traveled faster, it would be in the vicinity of the electron for a shorter amount of time, and hence the amount of transferred energy would be smaller.

This leads to an important note about how to choose detector thicknesses as described in [6]: *"Any detector that is to measure the full incident energy of charged particles must have an active thickness that is greater than the range of*

that particle in the detector material."

It is also worth noting, that particles of the same initial energy will not all deposit the same amount of energy in the same material. The path length of the individual particles of the same initial energy will vary and this effect is known as range straggling. The amount of range straggling affects the cutoff at the Bragg curve which describes the stopping power as a function of the distance of penetration.

Furthermore, energy straggling will also affect the deposited energy of a beam of monoenergetic particles. Energy straggling is the effect, that as the interactions for each particle traversing the detector will vary, the deposited energy will also vary. The amount of energy straggling is thus proportional to the width of the energy distribution of the particles traversing the detector.

1.1.2 Fast electrons (β^- particles)

When traversing matter, β particles can lose energy by Coulomb interactions with the orbital electrons in the same way as the heavy charged particles but they will also interactions with the nuclei much more often. Furthermore, they can also lose energy through radiative processes.

β particles lose energy at a significantly lower rate compared to the heavy charged particles, and they also differ from the heavy charged particles as they will not traverse the detector in a nearly linear path. Instead, they will follow a more serpentine-like path when traversing a material.

The curious reader would wonder why this is the case and what effects this might have. To explain this, remember, that β^- particles are electrons and therefore their mass will be equal to that of the orbital electrons of the detector materials. This has the consequence, that the β particles can lose a much larger fraction of their energy during each interaction. This way, a single interaction can have a drastic effect on the path of a β particle.

Furthermore, the β particles can also interact with the nuclei and this interaction can all of a sudden change the direction of a β particle considerably.

The last process that can cause β particles to lose energy is the radiative process bremsstrahlung or in general electromagnetic radiation. Bremsstrahlung is the effect that accelerated charges will radiate energy and as the β particles interact with the orbital electrons, they will be deflected which is essentially an acceleration. This effect will be largest for β particles with high energies and for detector materials with a large atomic number, Z.

The stopping power for β particles will then both contain the energy losses due to the collisions and due to the radiative processes, but the energy of the bremsstrahlung photons will on average be quite small.

An important thing to note is, that due to the serpentine pathway of the β particles, the understanding of range is less clear when we look at β particles. The penetration depth of a β particle will be noticeably shorter than the total path length of the particle.

To compare β particles with α particles, it should also be noted, that the specific energy loss of the β particles is much smaller and thus they will have a much larger path length. As a result, much thicker detectors are needed to detect β particles compared to α particles. Furthermore, both particles will also have larger stopping power in materials with a larger atomic number, Z.

As shown in figure 1.1, the stopping power of electrons in different materials can be seen as a function of the electron energy. Here it is seen, that the stopping power is clearly largest for electrons with lower energies and that the stopping power also increases for increasing atomic number. We will mainly be looking at particle energies ranging from 100 keV to 14 MeV and thus this figure does not describe the complete energy interval of interest.

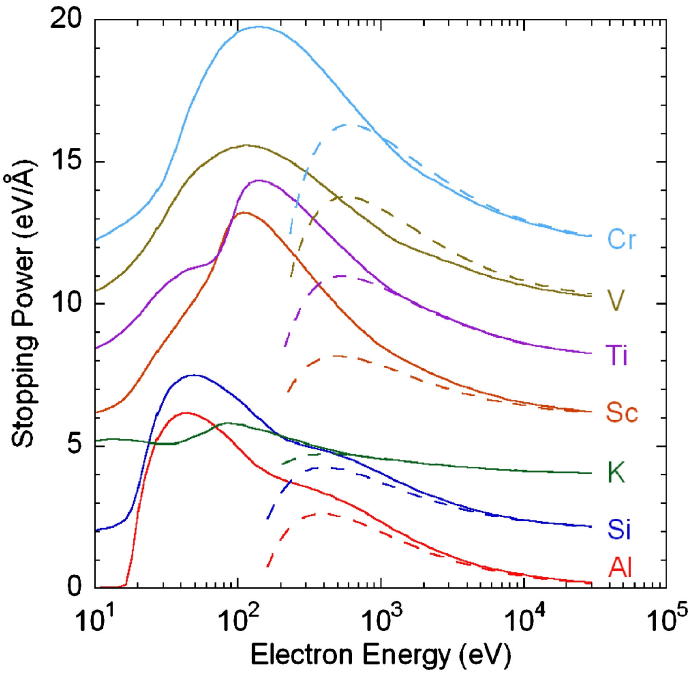

Figure 1.1: *"The solid lines show calculated SPs for Al, Si, K, Sc, Ti, V, and Cr as a function of electron kinetic energy E. The dashed lines show SPs calculated from the relativistic Bethe equation For clarity, the results for Si and successive elements have been moved upward in increments of 2 eV/Å." - figure and description has been reproduced from [11].*

1.2 ^{12}B as a β^- source

In this thesis, the β^- source, ^{12}B, will mainly be used to study the effects of backscattering in the setup. ^{12}B decays to ^{12}C through the β^- decay,

$$^{12}_{5}\mathrm{B} \rightarrow ^{12}_{6}\mathrm{C} + e^- + \bar{\nu}_e, \tag{1.2}$$

where an electron and an electron antineutrino are produced, when the mother nuclei decay into the daughter nuclei. As the interaction probability for (anti)neutrinos is very small, we will only be able to detect the electron - hence why we call it a β^- particle.

When the mother nucleus decays, the energy of the daughter nucleus will be close to zero and most of the released energy will go to the electron and the electron antineutrino. This means, that the energy of the electron can vary from zero and up to the Q-value of the decay and furthermore that the energy distribution of the electrons will be continuous.

The energy level diagram for ^{12}B can be seen in figure 1.2. Here, the Q-value for each of the allowed transitions is given together with the probability of each decay branch. In the energy level diagram, it can also be seen that ^{12}B only decays through β^- decay to the 0^+, the 1^+, and the 2^+ state of ^{12}C. This is due to the selection rules that secure conservation of angular momentum [10].

There are two types of decays; Fermi decays and Gamow-Teller decays. For Fermi decays, the spin is unchanged as the electron and the electron antineutrino couple to spin 0. For Gamow-Teller decays, they instead couple to spin 1. For ^{12}B, only Gamow-Teller decays are possible as Fermi decays are not energetically favorable.

The selection rule for Gamow-Teller decays tells us that $\nabla J = 0, \pm 1$. As $J_{^{12}B} = 1$, the equation calculating the possible angular momenta states that:

$$J_F = J_i - S, \tag{1.3}$$
$$J_i = 1, \tag{1.4}$$
$$S = 1. \tag{1.5}$$

When using the addition rules for angular momenta, this gives $J_F = 0, 1, 2$, and since the parity cannot change under a Gamow-Teller decay, ^{12}B can only decay to the three states $0^+, 1^+$, and 2^+ in ^{12}C which is consistent with the decay scheme in figure 1.2.

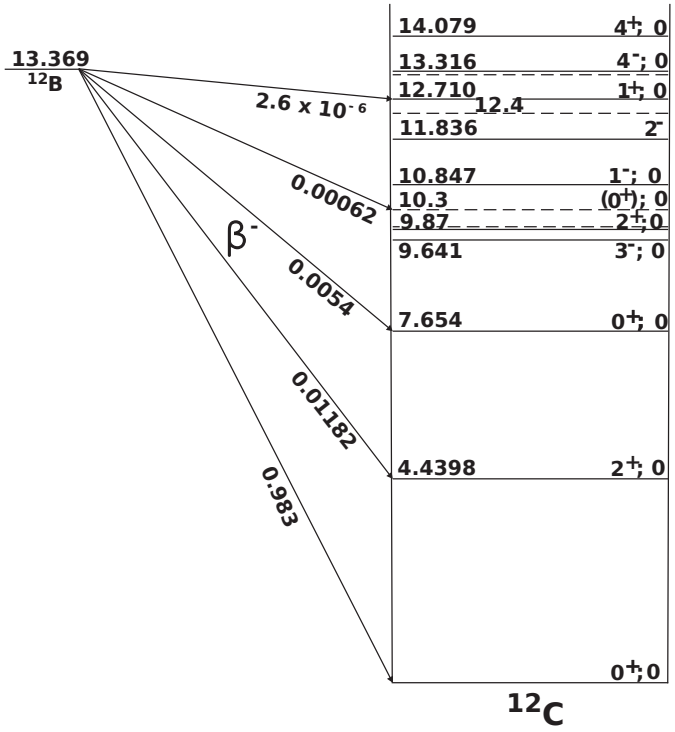

Figure 1.2: *The energy level diagram of the radioactive nuclei, ^{12}B, decaying through β^- decay to ^{12}C. The figure has been reproduced from [13].*

1.2.1 Backscattering

In this context, backscattering should be understood as the effect of a particle entering the detector and then at some point being scattered in such a large deflection angle that it escapes the detector again at the same or another surface roughly in the same direction as it originally entered the detector.

Backscattering can happen in all of the layers of the detector and as a result, some particles will be backscattered in the dead layers and others in the active layers. The particles being backscattered in the front dead layer will not be detected. When backscattered particles instead enters the active layer of the detector it will vary how much energy they will deposited in the detector before they are being backscattered. Thus, some of the particles will have deposited enough energy to be detected in the detector it was backscattered in and some will go unnoticed even though they actually had entered the active layer. This can possibly lead to a single particle being detected in several detectors, which can both affect the apparent intensity of the radioactive source and the apparent solid angle coverage of the setup. As an example, if we detect 1% more particles due to backscattering than what should actually be detected if backscattering

didn't occur, then we could be lead to think that the detectors had a larger solid angle coverage than what is actually the case. In addition, we could also blame it on the intensity of the source being larger than expected. Thus, backscattering can affect our understanding of other parameters.

Another thing to note is that the probability of a particle being backscattered varies with the energy of the particles. This means, that for β particles, the amount of backscattering will be larger for electrons of lower energy and for detector materials with high atomic numbers, Z.

1.3 Silicon detectors

Silicon detectors are a specific kind of semiconductor diode detectors and nowadays they are highly used detectors as they excel in some important areas. Semiconductor diode detectors have a superior energy resolution, they have a convenient compact size, and they have relatively fast timing. Furthermore, their thicknesses can be altered such that the detectors can be used for different requirements.

The detectors exploit the characteristics of a semiconductor to make an apparatus that is able to detect the energy of the particles. Essentially when a particle traverses the detector, electron-hole pairs are created along the path of the particle. By applying an electric field over the active region of the detector, these electrons and holes will move towards the contacts creating an electrical signal. The electrical signal can then be measured, and the deposited energy of the particle will be proportional to the pulse height of the electrical signal.

Below, the basic concepts of semiconductors and doping are described.

1.3.1 Semiconductors

In solids, energy bands describe the allowed energies of the electrons. Within a pure material, the electrons are confined to the energies within these bands. In some materials, these bands are separated by a range of forbidden energies. The size of this gap decides whether a material is a semiconductor or an insulator.

If there is a gap between the bands, we call the lower band the valence band and the upper band the conduction band. The valence band contains the electrons that are bound to a specific place in the lattice and thus cannot move freely around. The conduction band instead contains non-bound electrons, that are free to move. It is thus the electrons in the conduction band that contributes to the electric conductivity of the material.

In an intrinsic material without thermal excitation, there will not be any electrons present in the conduction band but the valence band will instead be full. If an electron from the valence band is excited enough to cross the

bandgap, it will instead occupy the conduction band and leave a vacancy in the valence band. Such a vacancy is called a hole, and the combination of the electron in the conduction band and the missing electron in the valence band is called an electron-hole pair.

By applying an electric field, these two charges (with the hole representing a positive charge) will drift in opposite directions both contributing to the conductivity of the material and thus the number of electron-hole pairs has an effect on the electric conductivity of a material. As a result, it is of interest to manipulate these concentrations by doping a material which is described in the next section.

1.3.2 Dopants

We now denote n as the concentration of electrons in the conduction band and p as the concentration of holes in the valence band. For an intrinsic semiconductor, the number of electrons in the conduction band will be equal to the number of holes in the valence band, and thus $n = p$.

Impurities in semiconductors can however change this property which can be exploited by purposely putting impurities in a semiconductor to alter its characteristics to the favor of the user. There are two different ways of purposely impurifying a material, which are described below.

n doping For this type of doping, the material will be doped with another material that has more valence electrons than the material itself. These extra electrons will be so lightly bound that they are easily excited to the conduction band. But as they are not bound to other atoms in the crystalline structure, this will not leave a hole in the valence band. The effect of these kinds of impurities are that the electrons in the conduction band outnumber the holes in the valence band largely. This way, the conductivity will almost exclusively be determined by the electrons and not by the holes. An examle of silicon doped with phosphorus can be seen at the left drawing in figure 1.3.

p doping For this kind of doping, the impurity instead has fewer valence electrons than the material itself. This leaves a covalent bond to be completed which then represents a hole. This hole can then be filled by normally excited valence electrons as this will not require as large excitation energy as if the electron should occupy the conduction band. These valence electrons will then leave a hole behind without creating an extra electron in the conduction band. As a result, the conductivity will almost exclusively be determined by the holes in the valence band. An example of silicon doped with boron can be seen at the right side of figure 1.3.

In general, this means that the dopants in doped materials shift the equilibrium between holes and electrons such that one becomes dominant with respect to

the conductivity of the material. For n+ and p+ materials, the impurities contribute to very high conductivity. The minority carriers will then allow such material to work as a blocking contact.

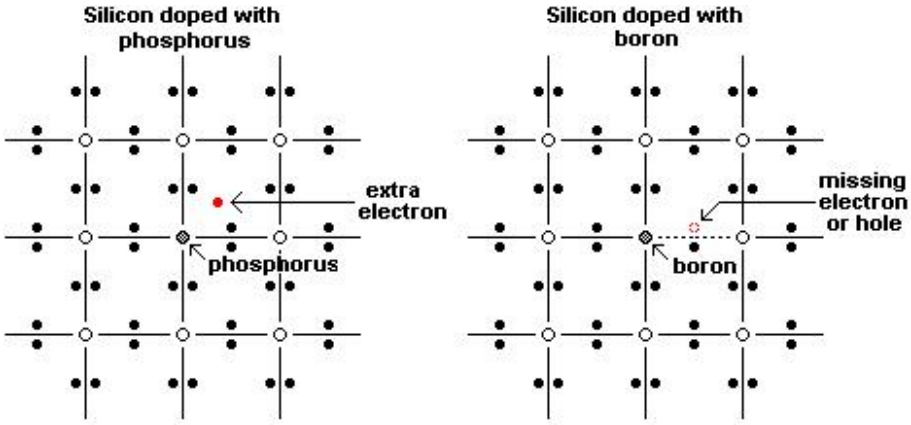

Figure 1.3: *The drawing on the left side shows an example of silicon being n-doped with phosphorus, and the right side of the drawing shows an example of silicon being p-doped with boron. The figure has been reproduced from [12].*

1.3.3 Semiconductor detectors

In semiconductor detectors, both p+ and n+ doped materials are used to make blocking contacts. This allows for detecting particles as an ohmic contact would not have been able to detect the increase in current coming from the particles due to the leakage current.

In this experiment, two kinds of semiconductor diode detectors will be used. A simple silicon pad detector and a double-sided silicon strip detector. The main idea with the strip detector is that compared to the pad will be able to detect both the energy and the position of a detected particle.

This is possible as the detector is divided into strips on the front and back side and the strips on the front side are orthogonal to those on the back side. When a particle traverses the detector and creates electron-hole pairs, these particles will travel along the field lines towards the contact of the strips they were produced in. The size of the signal in a strip will then depend on the number of charge carriers. As a result, we should only see a large signal in those strips, where the particles have deposited most of their energy. It is though possible for a particle to deposit energy in more than one strip giving a misleading signal.

A more detailed description of the structure of the detectors simulated in this thesis is found in section 2.3.

1.4 Simulated experiment

1.4.1 IGISOL

In this thesis, the main setup used for simulations was the setup used for experiments at the ION-Guide Isotope Separation On-Line (IGISOL) facility in Jyväskylä in 2020. IGISOL provides the user with the opportunity to produce low-energy radioactive beams, which can be used to study the properties of atomic nuclei.

The facility has an accelerator that accelerates a beam of ionized particles towards a thin target producing single charged particles. These particles are not stopped by the thin target, but they are instead stopped afterward by a Helium gas which does not change their charge. The combination of the target and the beam is chosen such that the production of ^{12}B is favored. After this, a mass separation is performed using a dipole magnet making sure that only particles of the same mass as ^{12}B is used. This will leave us with a collection of particles that does not only consist of ^{12}B but also ^{12}C etc. as no chemical separation is performed. At last, the particles are transported into the carbon foil in the setup making sure, that the particles are stopped in the foil and not transported further through the setup.

1.4.2 Experimental setup

Before this experiment was conducted, the Aarhus University Subatomic physics group (AUSA) did not have an experimental setup appropriate for the given task. The setup should be able to detect $\beta\alpha$- and 3α angular correlations in the β-delayed decays of both ^{12}B and ^{8}Li as described in [3]. This would require the setup to have a large solid angle coverage, and it should also be able to detect β-particles but at the same time have a high α-particle resolution.

Andreas Gad, who is currently a PhD student at AUSA, was responsible for designing a new setup meeting these requirements. The result was a 3D printed cube maximizing the solid angle coverage and holding the 12 detectors in place making sure the placement of them was consistent over time. The material of the 3D printed cube was chosen to be a nylon material (nylon PA12) making the setup able to be pumped down to 10^{-7} mbar.

Furthermore, the cube was mounted inside a cylindrical aluminum chamber to increase the γ resolution for future experiments. The experimental setup can be seen in figure 1.4b.

The detectors were chosen to be six W1 detectors, which are double-sided silicon strip detectors enabling high α-particle resolution. Behind each W1 detector, a thicker pad detector was placed making sure, that the setup can detect β-particles as well. This totals 12 detectors, but unfortunately one of

the pad detectors was defective, and therefore only 5 telescopes were fully functioning.

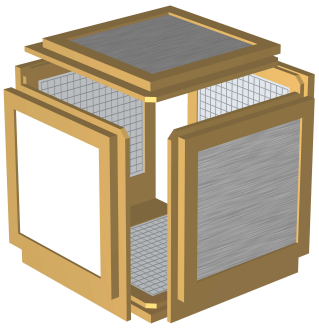

(a) *The drawing shows the placement of the 12 detectors placed in 6 telescopes. Each telescope consists of a double sided silicon strip detector (W1) with a pad detector behind it.*

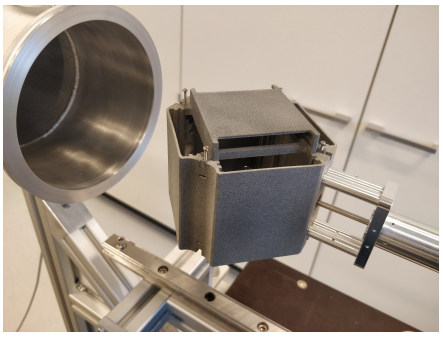

(b) *The picture shows the experimental setup used at IGISOL and it shows the cylindrical chamber, the placement of the beam, and the cube without the detectors in it.*

Figure 1.4: *The figures show the experimental setup used at IGISOL. The drawing and the picture has been reproduced from [3].*

Chapter 2

Monte Carlo Simulations in Geant4

In this thesis, the goal is to study the β^- response of the silicon detectors used by the Aarhus University Subatomic Physics group (AUSA). To do this, the Monte Carlo framework, Geant4 (GEometry ANd Tracking), has been chosen. A Monte Carlo toolkit allows us to simulate experiments with many degrees of freedom and it also allows us to fix some of these parameters. Therefore, using a Monte Carlo toolkit allows us to simulate situations with a large control over the parameters thus making us able to study effects that we cannot otherwise study in the laboratory.

Geant4 is developed at CERN and the framework is thus developed specifically for physicists studying particles traversing matter. The framework was hence an obvious choice for this project.

This chapter mainly has three parts. The first part explains the basics of Geant4 and what the user should provide to make a simulation using the toolkit. The second part of the chapter describes the program, G4Sim, which is a program using Geant4 developed at AUSA. The last part of the chapter then describes how the detectors, other things in the setup, and the sources have been implemented in this project.

2.1 Geant4

Geant4 specializing in simulations of particles traversing matter. It is therefore highly applicable in the parts of nuclear physics where we study particles traversing detectors and other materials in the setup. Geant4 is a framework, that is built upon C++ and it is thus an object-oriented framework. It has several different classes taking care of different parts of the simulations where some of these things should be specified by the user. More specifically, the user will at least have to specify the following things characterizing the specific simulation:

- The geometry of the detectors

- The particle source
- How to detect particles, and which data to save from an event
- The physics processes
- The main method

In Geant4, an experiment is carried out as a run starting with the command `beamOn`. Within a run, the settings are constant and so the user can not change the geometry or other settings during a run. A run consists of a collection of events and an event carries information about the particles, hits, and all of the trajectories, etc.

The movement of a particle can then be described by steps. A step should be seen as the "delta" information of a particle moving from one poimnt to another. A step consists of two points, and it carries information of the energy loss, the ToF spent by the step, etc. A step also knows the starting volume and the end volume of the particle.

The current information of a particle is then described by a track. A track can be seen at a *snapshot of a particle* and it contains the position of the particle and all of the physical quantities of the particle at the given time and position.

All of these things make it possible to simulate particles traversing matter and to extract data to examine the results of a simulation [2]. Apart from this, Geant4 also offers a built-in unit system. It comes with all of the most common units and you can also define your own units. This makes it easy to be consistent and eliminates unit errors.

In the following sections, how to specify the characteristics of a simulation will be described. More specifically, four of the points mentioned above will be described in more detail.

2.1.1 Geometries

When making the complete geometry of a single detector, the detector is divided into separate parts and these are made individually. When making these parts, the user should specify which geometries are "active" volumes where the particles are detected. Volumes, which are not declared as active volumes, only act as materials where particles can be scattered and lose energy. All of these separate parts will together give us the detector with the dead layers and the active layers.

When starting to make a geometry in Geant4, a world volume should be created and all of the parts of the setup should be placed in this world. Each volume should be given a mother volume, and this can either be the world volume or another volume that is recursively placed in the world volume. As an example, this can be used to make a volume for each detector to be placed in.

When making a part of a detector, the name, the dimensions, and the material should be defined. After making a single volume of a detector, the volume should be placed, and here you should define the rotation, the placement, and the mother volume amongst other things. A volume can be placed several times if the volume should have the same dimensions and material. To make visualization easier, you can also define the color of a volume.

When rotating elements in Geant4, you should be very careful. When you place an element with a non-zero rotation, you should be aware, that the defined axis of rotation is defined in accordance with the element itself. If you want to rotate the element with respect to the central coordinate system, you should further rotate the element. This can be done by rotating the coordinates with respect to this central coordinate system before placing the element. This gives you the option of both rotating an element with respect to its own coordinate system and with respect to the central coordinate system. When doing these rotations, it is very easy to slip up, and it is thus highly recommended to use the visualization tool during the process to eliminate errors.

2.1.2 Particle source

There are several different options when making a particle source in Geant4. The framework gives you different options including the `G4GeneralParticleSource` which has been the primary source in this project. When making a particle source, you should specify the following, but there are many other options:

- Particle type
- Energy distribution
- Position of origin
- Direction / angular distribution

If you choose the general particle source, all of these settings can be set in the macro file, which you can run to start a simulation. Thereby these things can be changed after compilation which is an advantage.

2.1.3 How to detect particles

When making the setup, you should, as mentioned above, define which volumes are active volumes. These will be the volumes where you can detect particles. Furthermore, you should also define which data to save when a particle is detected. Here, you can for example save the volume it was detected in, the energy of the particle, the angle the particle entered the volume in, etc. In these simulations, it has been a focus, that the extracted data should be as

close to the data that we can extract from the real experiment. Therefore, only positions and energies have been collected for each event.

When saving this data, you can also further sort the data. Here, you can for example implement a threshold simulating that the real setup is not able to detect particles with energies below some given threshold due to the electronics in the setup.

2.1.4 The physics processes

The physics in Geant4 are controlled by a process class [1]. This class defines how particles of different types should interact. There are three different groups of processes; electromagnetic, hadronic, and decay/reference processes. Geant4 provides several different predefined physics lists which are implementations of these processes[1].

In this project, the electromagnetic physics processes was changed from EmLivermore to EmOpt2 as the package stated that it clearly also covers processes also at lower energies for electrons and positrons.

2.1.5 Visualization

Geant4 offers several different choices of visualization drivers, and each of them offers different advantages. Throughout this project, `openGL` has simply been used . This tool comes with several different options and it will amongst other things enable you to see the setup, rotate it, see the different layers and see particle tracks. Therefore, this is a very powerful tool to double-check your work.

No matter which driver you choose, I cannot stress enough how important it is to use the simulation tool frequently. It will save you from foolish mistakes, and therefore I will clearly recommend always double-checking your things using a visualization tool.

2.2 G4Sim

G4Sim is a program made mainly by Andreas Gad from the Aarhus University Subatomic physics group (AUSA). It implements a Geant4 project tailored to the systems and detectors used by the group.

[1] If this has your interest, you can find a complete list of the different predefined physics lists at this webpage: `https://geant4-userdoc.web.cern.ch/UsersGuides/PhysicsListGuide/html/index.html`.

The program implements two different kinds of silicon detectors; a pad detector, and a double-sided strip detector. The program uses AUSALIB [4], which is a program made by AUSA. AUSALIB enables G4Sim to get information on the detectors from a JSON file. This way, the user can easily make different detectors of the same type only by changing the specifications in the JSON files. This is a huge advantage as this can be changed after compilation.

The program also reads a setup file where you can define the placement of the detectors in the setup. This way, the placement of several detectors is also read at runtime which again ensures that it can be changed after compilation.

In G4Sim, the output format is chosen to be the root format. This way, the data files can be easily examined using the root library. This also enables the program to output data files of the same structure as data files from the original experiment.

When making G4Sim, it was chosen that the double-sided strip detector, W1, should be implemented with 16×16 pixels. This way, the program detects which pixel a particle was detected in. In the real experiment, we can only know the number of detected particles in each of the 16 front and back strips. As a result, the simulation can provide us with information, that is normally unavailable to us. To make the experiment and the simulation more comparable, the hit data of the simulations are modified before saving the data by converting the pixel hits into strip hits. In this process, an energy threshold is also implemented emulating the threshold of the real experiment. In the original version of G4Sim, the double-sided strip detectors only consisted of a front dead layer, a back dead layer, and the 16×16 pixels.

The pad detector has a much simpler design. Therefore, these were only made up of three elements; the front dead layer, the active layer, and the back dead layer.

My addition to the program has been to further implement the fine structure of the two kinds of detectors and to make sure it functions with AUSALIB. Furthermore, I have also implemented other parts of the setup which are expected to contribute to backscattering. Thereby, my additions to the program enable us to study backscattering in a much more detailed setup. Screenshots of the full implementation can be seen in figure 2.7.

2.3 Implementing the detectors

When implementing the detectors, we chose to keep the skeleton originally provided by G4Sim. This means, that the implementations should support AUSALIB, which reads the detector information from JSON files. A screenshot of the simulated detectors can be seen in figure 2.7a.

2.3.1 The silicon pad detector

The pad detector is the simplest detector and it consists of a front dead layer, an active layer in the middle, and a back dead layer. The front and back dead layers can be of different thickness, and the detector has a square form.

The pad is simply implemented with an aluminum front dead layer, an active layer of silicon, and a back dead layer of aluminum. A sketch of this simple design can be found at figure 2.1. To make the user able to locate the front of the detector when using the visualization tool, the front and back dead layers are given different colors. The specifications of the 6 pads used in the experiment and in the simulations are given in table 2.1. Note, that pad-2 was, unfortunately, malfunctioning in the experiment and therefore, no data could be collected with this detector.

Pad #	Active layer	Name at AUSA
1	1036 µm	AUPAD_1000_3112-16
2	1036 µm	AUPAD_1000_3221-16
3	1497 µm	AUPAD_1500_3289-4
4	1490 µm	AUPAD_1500_3289-5
5	1498 µm	AUPAD_1500_E11
6	1038 µm	AUPAD_1000_3112-14

Table 2.1: *The information on the pad detectors used in the experiment and in the simulations. Note that in the experiment, pad-2 was malfunctioning, therefore no data could be extracted from this pad. All of the detectors have a front and back dead layer of thickness* 500 nm*, and the dimensions of all of the pads were* 5 cm*.*

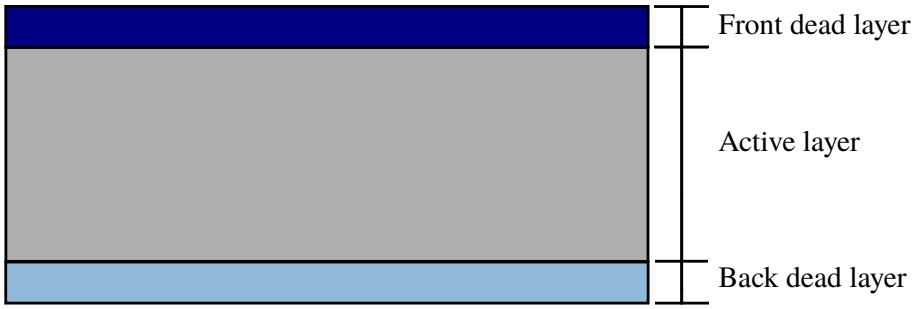

Figure 2.1: *The sketch depicts the simple layout of the pad detector. Note, that this is only a sketch and thus does not have any scaling ratio. You should thus be aware that the sizes at the two axes are skewed.*

2.3.2 The W1 detector

In the experiment, six double-sided strip detectors of the type W1 were used. This type of detector has a way more complex design compared to the pad detector. The design of the W1 can also be divided into three sections; the front dead layer, the active layer of silicon, and the dead layer on the back side of the detector. But in contrast to the pad detector, each of these three sections has a fine structured design which will be described in the following paragraphs.

The detector is a 16×16 strip detector with 16 front strips and 16 back strips. At the front side, the strips are vertical, and at the back side, the strips are horizontal. The strip numbering at the front increases from left to right and at the back, the strip numbering increases from top to bottom.

To make it more painless for the user to navigate in the visualization tool, I have colored the top left corner on the front side of the W1 red corresponding to strip (1,1), and the top right corner corresponding to strip (1,16) has been colored blue. A green marking then shows the two middle front strips in the 1st back strip at the front side of the detector corresponding to pixels (1,8) and (1,9). This way, it is possible to determine where the different strips are placed and where the front/back of the detector is placed when using the visualization tool. A drawing of the front and back layout of the detector can be seen in figure 2.2.

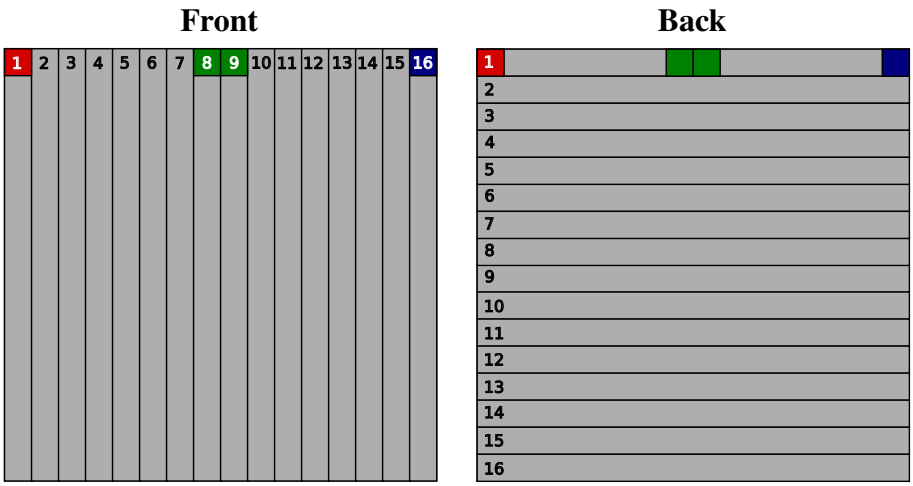

Figure 2.2: *Sketch of the general design of the W1 detector. To the left, the design of the front side is seen and to the right the design of the back side is seen from the front of the detector. Note the placement of the colored squares indicating the strip numbering for easier positioning using a visualization tool.*

Active layer

The active layer consists of a single silicon box in real life. To simulate that the particles can be detected in one of the 16 front strips and in one of the 16 back strips, we instead use another approach in the simulation. Here, the active layer consists of 16×16 boxes of silicon. These boxes lay side by side with no holes in between them. They have the width of the *strip pitch* which is the strip width plus the width of two halves of the SiO_2 boxes. This way, the detector will have the width of $16 \times$ *strip pitch* and it will be quadratic. The active layer will therefore fill the detector all the way out to the edges and at the edges.

When choosing this approach, concerns were made that this would be too ineffective and that this could not solve the problem of sharing events correctly. However, the library, AUSAlib [4] is able to sort the sharing events if this is to be of importance in the future. Furthermore, this version of the design had also already been made by a phD student, S. Viñals, resulting in an article [14] and she did not mention any performance problems choosing this design.

Dead layer on the front side

Each front strip will follow the design sketched IN figure 2.3. The figure shows that each front strip consists of a layer of p+ doped silicon and boxes of SiO_2 that separates these doped layers making sure, that these strips are isolated from each other. On top of each strip, three aluminum contacts are placed; one in the middle and two at a specific distance from the edge of the doped layer. This distance is named the *end of strip length* and it is expected to be a constant value decided by the equipment used to produce the detectors when they layer and corrode the materials. The design using these three small contacts is part of a newer design minimizing the thickness of the dead layer on the front of the detector and thereby decreasing the effect of the dead layer on the deposited energy.

In the simulations, all of the boxes in the front dead layer are not set as active materials. This means, that these parts of the detector only act as a dead layer where the particles can be scattered and deposit energy. Therefore, no particles are detected here. Furthermore, the p+ doped layers were approximated by normal silicon.

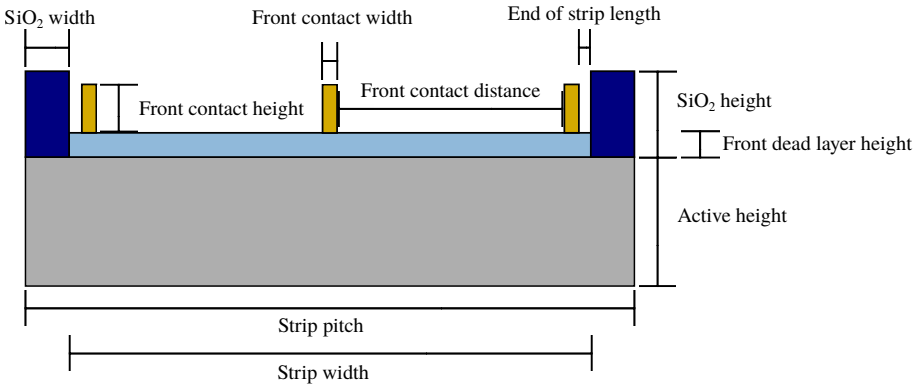

Figure 2.3: *A sketch of a single strip of the front side of the W1 detector. Note that this is only a sketch and therefore the sizes are skewed. A more detailed description of the design can be found in the text.*

Dead layer on the back side

The dead layer on the back side of the W1 detector has a quite similar design as the front side, it is however n+ doped instead. The structure of the dead layer also differs in the way, that it only has one broad aluminum contact for each strip. This is reasonable, as it is not as important to minimize the dead layer on the back side of the detector as on the front side of the detector. The distance between this layer of aluminum and the oxide strips is again assumed to be the same value as on the front side as this distance depends on the way the detectors are produced.

Note, that we was not able to find a former drawing of the back side of the detector neither from the producer nor from the libraries at AUSA. A drawing of the design of the back side of the detector is depicted in figure 2.4.

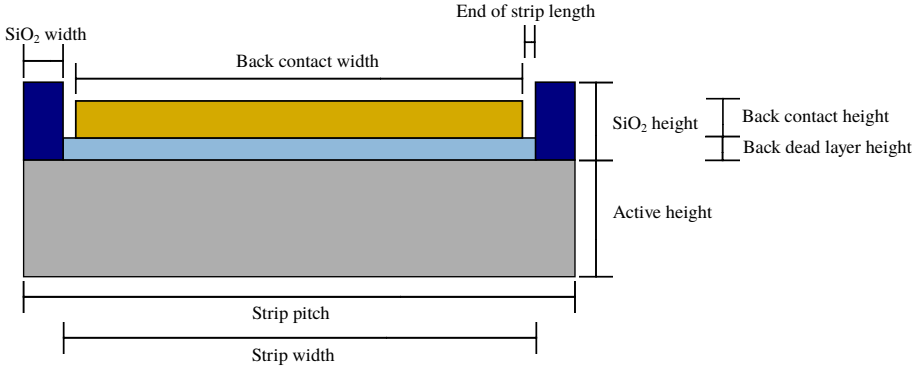

Figure 2.4: *A sketch of the design of a single back strip of the W1 detector. note, that this sketch does not follow a specific scale ratio and therefore, the sizes are skewed. A more detailed description of the design can be found in the text.*

Measurements of the W1 detectors

The general measurements of the W1 detectors are given in table 2.2, and the meanings of the names can be seen in figures 2.3 and 2.4. The specifications that differ for each detector are then given in table 2.3.

Name	Measurement
Active height	Differs for each detector
Strip width	3120 µm
Strip pitch	3220 µm
SiO2 height	0.6 µm
SiO2 width	100 µm
End of strip length	15 µm
Front dead layer height	100 nm
Back dead layer height	0.4 µm
Front contact height	0.2 µm
Front contact width	30 µm
Front contact distance	1500 µm
Back contact height	0.2 µm
Back contact width	3090 µm

Table 2.2: *General measurements of the W1 detectors. The meanings of the names can be seen in figures 2.3 and 2.4.*

Detector #	Active layer	Name at AUSA
1	67 µm	AUW1_60_2881-1
2	1002 µm	AUW1_1000_2541-7
3	65 µm	AUW1_60_2887-4
4	60 µm	AUW1_60_3187-5
5	60 µm	AUW1_60_DSSD-7
6	1043 µm	AUW1_1000_2947-4

Table 2.3: *Individual information on the W1 detectors that has been used for the simulations and in the experiment at IGISOL.*

2.3.3 Placement of the detectors

The placement of the detectors is determined by the layout of the 3D printed cube. The four pads and W1s on the sides of the cube are placed symmetrically and the detectors on the bottom/top of the cube are also placed symmetrically. The placements of the detectors are described in table 2.4 by the distance from the center of the cube to the center of the detectors.

	Distance from center
W1 side	42 mm
W1 top/bottom	40.5 mm
Pad side	46.95 mm
Pad top/bottom	45.5 mm

Table 2.4: *The placement of the different detectors is given. Note, that the placement is defined as the distance from the center of the cube to the center of the detector itself.*

2.4 Implementing other things in the setup

In the actual setup, there are many other things present than the detectors themselves. Each detector is mounted in a frame with wiring and each of these frames is mounted in a 3D printed cube ensuring a consistent placement of all of the detectors. This cube is placed inside a tube where all of the wirings also runs.

All of these parts of the setup are expected to contribute to the scattering of particles and therefore the most obvious sources of scattering are simulated these being the frames of the detectors, and the 3D printed cube. In the next section, it is described how these parts of the setup were approximated.

2.4.1 Detector frames

A sketch depicting the approximated frames of the pad and of the W1 detector can be seen respectively in figure 2.5a and figure 2.5b. These frames were simulated using a flag thereby enabling the user to easily change this flag deciding whether the frames should be included in the simulations or not. This enables the user to make simulations with and without the frames and thus, the user will be able to compare the two situations.

The frames were made of the material FR-4, which is a glass-reinforced epoxy laminate material[2] and the same material was used for the simulations. The measurements of the frames are given in the figures - note that the two frames are identical except for the bottom part. furthermore, a screenshot of the simulated detectors with the frames can be seen in figure 2.7b.

[2]You can read more about the material at `https://en.wikipedia.org/wiki/FR-4`.

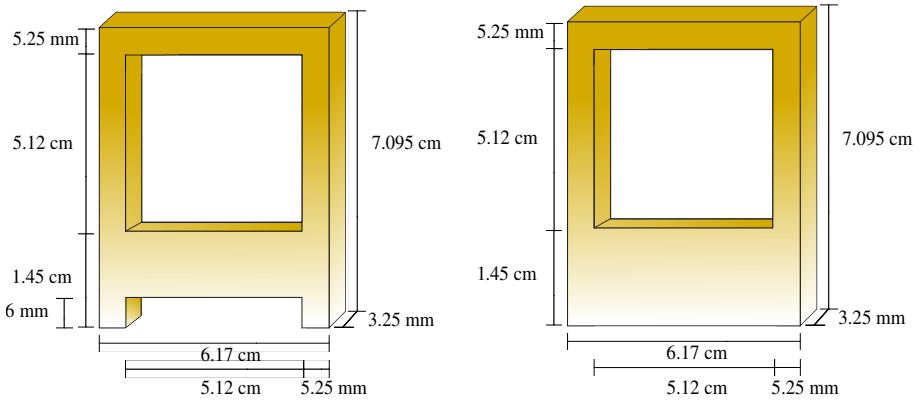

(a) Frame for the pad detector. *(b) Frame for the W1 detector.*

Figure 2.5: *The drawing depicts the frames for the pad and for the W1 detectors. Note, that the two frames are identical except for the bottom part. You should further note that the sketch does not follow a specific scale ratio. A more detailed description of the implementation of these frames can be found in the text.*

2.4.2 The Cube

The 3D printed cube had a very complex design. Therefore, it was approximated using 6 different boxes; a box for the top and bottom wall, a box for the four walls at the sides, a box approximating the corner trapezoidal cylinders, and 3 different boxes approximating the frame which lies close to the top and bottom wall. The corner trapezoidal cylinders were approximated using a box with the approximately same cross section as the original corners. Drawings of these boxes including the measurements can be seen in figure 2.6. The material of the cube is made out of nylon PA12 but as nylon PA11 was predefined in Geant4, this material was used instead.

Furthermore, these elements had to be placed correctly with respect to the center of the setup. To do this, the elements were placed in the following way:

- The center of the side box was placed 5 cm from the center of the cube.
- The top and bottom boxes were placed 5 cm from the center of the cube again measuring from the middle of the two boxes.
- The top frame was placed such that the top of the frame was parallel with the top of the side boxes. The same was the case for the bottom frame just mirrored.
- The corner boxes were placed 5.655 cm from the center of the cube again measuring from the center of the corner box.

When simulating the elements of the cube, one should be especially aware of the coordinate system and how to rotate the elements correctly. The coordinate system is arranged in such a way, that the xz-plane is parallel to the large side of the top box of the cube and the two axes point towards the corner boxes. The y-axis is then orthogonal to the xz-plane.

This noteworthy coordinate system makes the side boxes and the frames exceptionally hard to place correctly as these elements should both be rotated around the center axis of the cube but also around their own axis. The corner boxes and the top/bottom boxes should only be rotated around their own center axis and hence these are more effortless to place. Screenshots of the simulated cube from the corner and from the top can be seen in figures 2.7c and 2.7d.

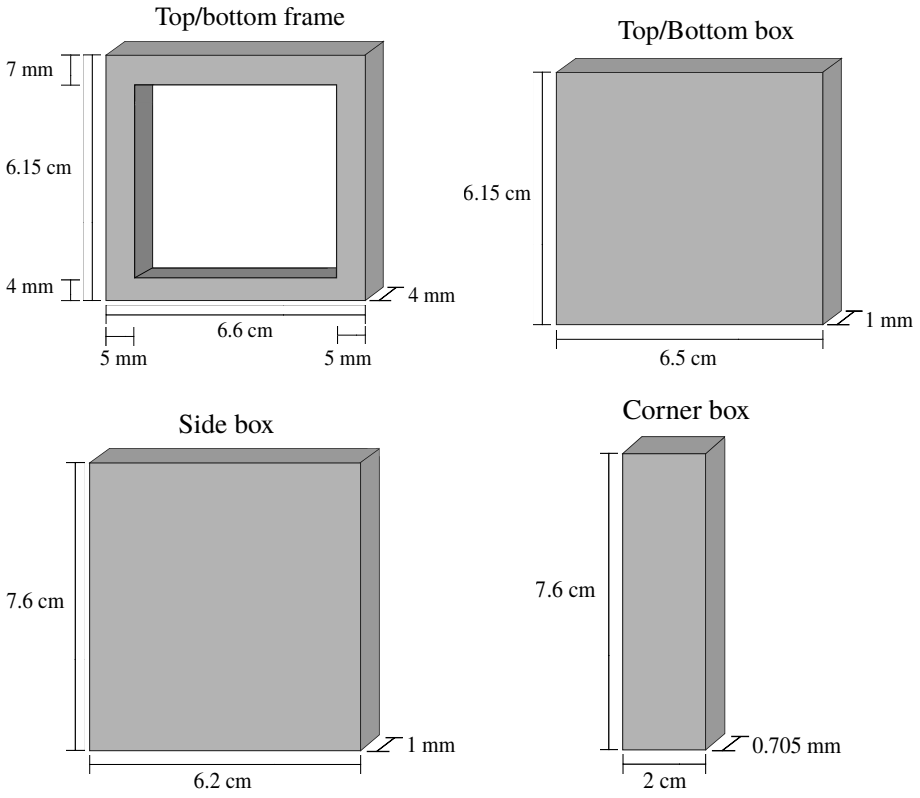

Figure 2.6: *The sketch shows the different boxes that together approximate the structure of the 3D printed cube. Note, that the top/bottom frame is made out of three different boxes. Therefore, 6 different boxes have been used to simulate the cube. A more detailed description of the implementation of the cube can be found in the text.*

2.5 Implementing the sources

In the simulations, two different sources have primarily been used. The first one is a very simple monoenergetic point source dispatching particles in either a predetermined direction or with an isotropic angular distribution. This source has been used with both α and β particles but primarily with β particles. The other source is a more sophisticated source recreating the energy distribution of the e^- and the $\bar{\nu_e}$ from the decay of ^{12}B decaying through β^- decay to ^{12}C. Furthermore, this source was not a point source abut instead a plane circle with radius 0.45 mm.

In the four subfigures in figure 2.7, this decay has been simulated. Here, the red line indicates the track of the e^-, and the gray line is the track of the $\bar{\nu_e}$.

Both these sources have been made using the general particle source (GPS) in Geant4. This way, the choice of particle source could simply be set in the macro. The more sophisticated source was made using the ion function of the GPS. This creates the given ion (A, Z) and decays the ion making sure that the correct energy distribution is made using a data file for this. If the ion should be able to decay, it is however important that you remember to include the decay package. This can simply be done by adding it to the physics list using `physicsList->AddDecays()`.

Furthermore, the ion function has also been used to make a $^6_2$He source for checking the effects of backscattering. A simulation with a $^8_3$Li source decaying through β^- to $^8_4$Be, which then decays to two α particles has also been made. This simulation was produced for another master student writing his thesis at the group looking at the angular correlations of these particles.

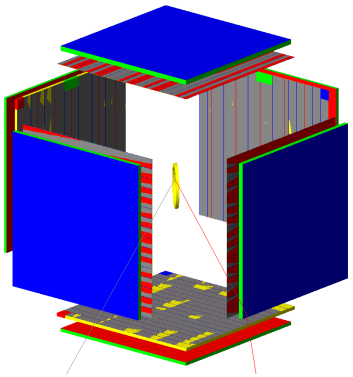

(a) Simulation with the 12 detectors present.

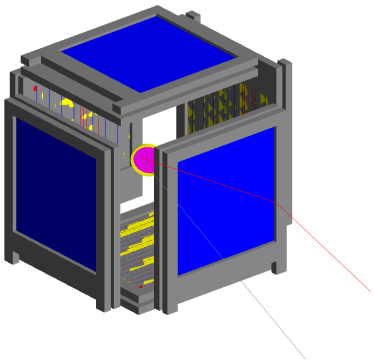

(b) Simulation with the 12 detectors and their frames present.

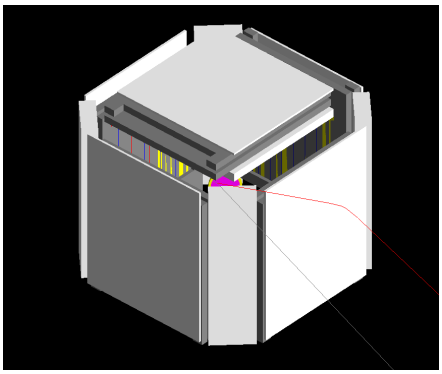

(c) Simulation with the 12 detectors, their frames, and the cube present.

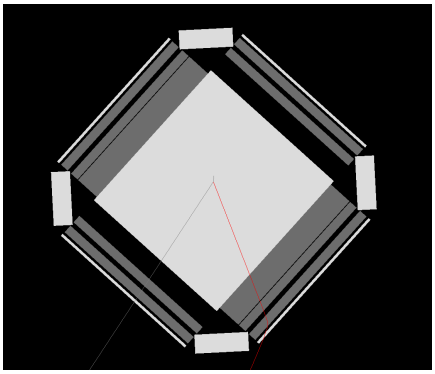

(d) Simulation with the 12 detectors, their frames, and the cube present.

Figure 2.7: *Screenshots from the visualization program depicting the setup. In all of the four simulations, we see the decay of* ^{12}B *decaying through* β^- *decay to* ^{12}C*. Note, that the red line indicates the track of the* e^-*, and the gray line is the track of the* $\bar{\nu_e}$*.*

Chapter 3

Simulations with G4Sim

The process of simulating the complex experimental setup used at IGISOL was divided into three main parts. The first part of simulating the setup was testing whether the implementation of the detectors works correctly. After this, different effects were studied using simple monoenergetic sources and at last, realistic sources was used to produce data and results that should be comparable with the real experiment performed at IGISOL . In this chapter, the same structure has been chosen thereby enabling the reader follow to our mindset of choosing the relevant simulations and figures to perform and display.

When performing the simulations, mainly two sizes of simulations have been performed; simulations with 1 million particles and simulations with 10 million particles. Using a computer with a 2.7 GHz dual-core Intel Core i5 Broadwell processor and 8 GB memory[1], the small simulations took around 5-10 minutes and the long simulations took 20 minutes to 1.5 hours. For comparison, simulations with 100,000 particles could be completed in less than a few minutes.

As a side note you should be aware, that the counted number of particles has been approximated by a Poisson distribution and therefore the uncertainties on the number of counted particles has been approximated by $\sqrt{n}$, where n is the number of counted particles.

3.1 Testing and checking

An important aspect of writing good code is to test the code thoroughly to make sure it works as intended - a running program might still contain some critical errors which can affect the final conclusions. When doing simulations with the purpose of exploring new effects, testing is especially important as we are not able to compare with previous results. Here, we can't always know whether the results yield critical errors in the code or if they yield physical effects that we are only able to see when using simulations. Thus, an important part of the simulation process has been to check that everything is working as

[1] The specification of the computer can be found at at apples website: `https://support.apple.com/kb/SP715?viewlocale=en_US&locale=da_DK`.

expected. The testing has mainly been done by making sure the simulations reproduce known physical effects and these physical effects will be discussed in this section.

3.1.1 Energy deposited by β^- particles

At first, the energy deposited in the detectors by electrons was examined by looking at the energy spectra of the deposited energy. In our simulations, we roughly have four categories of detectors; a thin W1, a thick W1, a thick pad, and a thinner pad. Therefore, the energy spectra were studied for all of these four detector types. To do this, a simulation with 1 million 5 MeV monoenergetic electrons with an isotropic angular distribution and only the detectors present was used.

The expected deposited energy of 5 MeV electrons in silicon has been calculated for comparison. The stopping power of 5 MeV electrons in silicon is given by $1.758\,\mathrm{cm}^2/\mathrm{g}$ [8] and the mass density of silicon is given by $2.33\,\mathrm{g/cm}^3$ [9]. Using these values, the expected deposited energies have been calculated:

$$\begin{aligned} E_{65\,\mu\mathrm{m}} &= 26.6\,\mathrm{keV}, \\ E_{1002\,\mu\mathrm{m}} &= 410.4\,\mathrm{keV}, \\ E_{1036\,\mu\mathrm{m}} &= 424.4\,\mathrm{keV}, \\ E_{1497\,\mu\mathrm{m}} &= 613.2\,\mathrm{keV}. \end{aligned}$$

As the four subfigures in figure 3.1 show, the expected values do not match the mean values of the histograms perfectly - but they do come very close. When comparing the expected values with the mean value of the histograms, it should be noted that the mean value might be skewed due to the characteristics of the spectra of the deposited energy. Thus, we would actually expect the mean value not to match the expected value precisely due to the characteristics of the spectra.

The characteristics of the spectra can be divided into three main parts; a peak which is very steep towards lower energies, a long tail to the right of the peak, and a plateau at small energies. These characteristics occur as every single β particle will not deposit the same amount of energy due to the processes described in section 1.1.2. The reason for the large tail towards higher energies and the steepness of the peak towards lower energies should be found in the way that the particles deposit their energy. Electrons deposit their energy in many interactions, and the probability that all of these encounters result in a minimal energy transfer is much smaller than the situation where at least some of the interactions result in a large energy transfer which causes the large tail towards higher energies.

The reason for the plateau at smaller energies is that not all of the particles will deposit all of their energy in the detector. These particles could possibly be particles going through the corner of the detector, particles being backscattered, or maybe particles depositing the main part of their energy in one strip but the

rest in another strip. To understand the exact processes causing the plateau at smaller energies, further studies would have to be made.

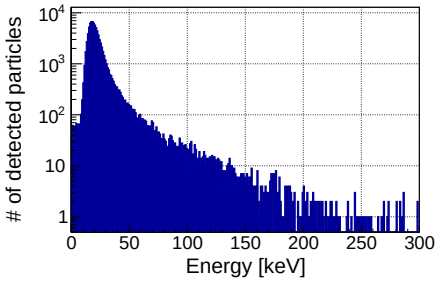

(a) *Energy distribution of* 5 MeV *electrons depositing energy in detector W1-3 which has an active layer of* 65 µm. *The mean value of the spectrum is* 23.46(6) keV.

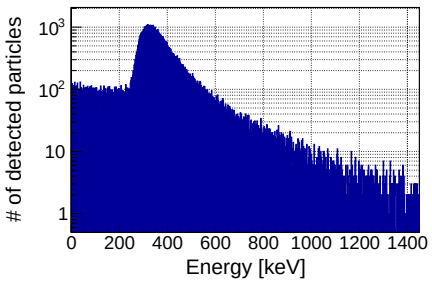

(b) *Energy distribution of* 5 MeV *electrons depositing energy in detector W1-2 which has an active layer of* 1002 µm. *The mean value of the spectrum is* 363.60(54) keV.

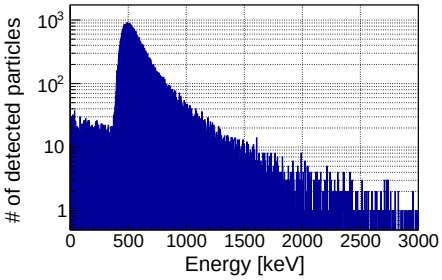

(c) *Energy distribution of* 5 MeV *electrons depositing energy in pad-3 which has an active layer of* 1497 µm. *The mean value of the spectrum is* 606.80(97) keV.

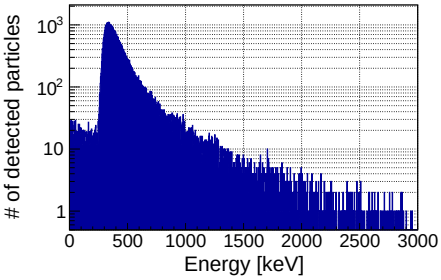

(d) *Energy distribution of* 5 MeV *electrons depositing energy in pad-2 which has an active layer of* 1036 µm. *The mean value of the spectrum is* 454.50(94) keV.

Figure 3.1: *Energy distributions of* 5 MeV *electrons depositing energy in four different detectors; two pads and two W1s all with active layers of different thicknesses. A description of the characteristics of the energy distributions can be found in the text. For the W1 detectors, the energy distribution is from the electrons detected in the front strips.*

3.1.2 Energy deposited by α particles

To check the response of heavier particles, the energy deposited by α particles was also studied. A simulation with 1 million 5 MeV α particles with isotropic angular distribution and only the detectors present was made for this purpose.

The stopping power of α particles in silicon is given by 616.2 cm^2/g [7] and the mass density of silicon is given by 2.33 g/cm^3 [9]. Using these values, the expected energy deposited by α particles in two detectors of different thicknesses has been calculated for comparison with the simulation:

$$E_{65\,\mu m} = 10\,\text{MeV},$$
$$E_{1002\,\mu m} = 154.4\,\text{MeV}.$$

From this, we can see, that we should expect the particles to deposit all of their energy in the front detectors as even a thin W1 will stop the particles. This can also be seen in figure 3.2 as there is a large peak just below 5 MeV which is probably due to the particles losing a small amount of their energy in the front dead layer before depositing energy in the active layer of the detectors. Furthermore, one should also note the smaller peak at lower energies. This is expected to be caused by the particles entering the detector through some of the areas with a thicker dead layer such as the front contacts or the SiO_2 layers as these would be expected to have a smaller amount of energy to deposit in the active layer of the detector.

Note, that as a result of the particles depositing all of their energy in the front detectors, α particles are not detected in the pads when using telescopes with W1s as front detectors and pads as the backing detectors.

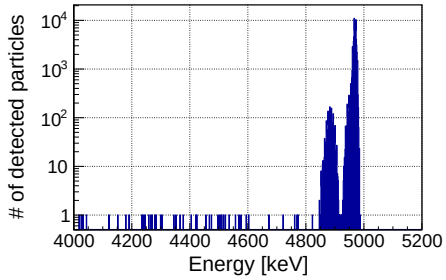

(a) *Energy deposited by* 5 MeV α *particles in the front detector W1-3 which has an active layer of* 65 µm.

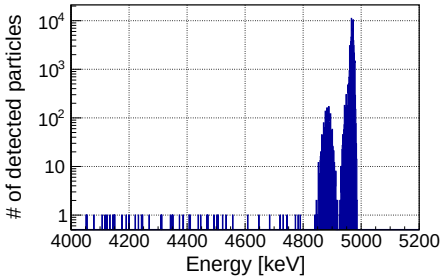

(b) *Energy deposited by* 5 MeV α *particles in the front detector W1-2 which has an active layer of* 1002 µm.

Figure 3.2: *Energy distributions of* 5 MeV α *particles depositing energy in two different W1s with different active layers. Note, that as the particles deposit all of their energy in the front detectors, they are not detected in the pads and therefore the energy distributions in the pads are not depicted. A description of the characteristics of the energy distributions can be found in the text.*

3.1.3 Angular effects

It is a well-known effect that a source sending out particles with isotropic angular distribution will not be seen as having an isotropic distribution from a plane observing the source. Directly in front of the source, more particles are expected to be seen, and at larger angles, fewer particles should be seen. Therefore, the expectation is that the W1 detectors will detect more particles at the middle strips (strips 8 and 9) compared to the strips at the edges when the source is placed in

the middle of the setup. It should also be noted, that this should hold for both the vertical and the horizontal strips and thus both for the front and back strips.

To test this effect, the simulation described in section 3.1.1 has been reused. The number of detected particles has been plotted as a function of the front and back strip number which can be seen in figure 3.3. Here, it can be seen that the effect of the isotropic source being placed in the center of the setup is very prominent. Comparing the number of detected particles in the middle strips to the number of detected particles in the outermost strips, only approximately around 65% are detected in the outermost strips compared to the middle strips. This is thus a prominent effect that is clearly seen in the simulations.

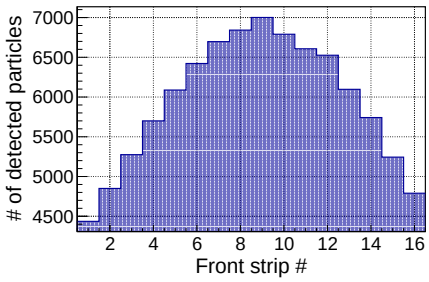

(a) The number of detected particles is shown as a function of the front strip number for the detector W1-4.

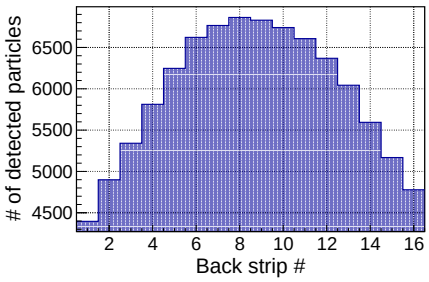

(b) The number of detected particles is shown as a function of the back strip number for the detector W1-4.

Figure 3.3: *The number of detected particles in a W1 detector is shown as a the function of front and back strip numbers respectively for a monoenergetic* 5 MeV *electron source with isotropic angular distribution. The effect of the isotropic source being placed in the center of the setup is clearly prominent. A more thorough description can be found in the text.*

Another angular effect is expected to appear in the deposited energy as a function of the strip number. This is due to the fact that if the source is placed in the center of the setup, the particles traversing the outermost strips will traverse a longer path through the detector compared to the particles traversing the detector in the middle strips. The particles traversing the detector at larger angles are thus expected to deposit a larger amount of energy compared to those traversing the middle of the detector.

To study this effect, 16 simulations each with 1 million monoenergetic 5 MeV electrons were made. Only the detectors were present in these simulations and for each simulation, the source was pointed towards a single strip. This way, the primary response was in a specific strip. It did, however, turn out to be difficult to determine precisely if the middle of a given strip was hit - the visualization tool especially failed to help at larger angles. Therefore, the energy distribution in the strips had to be used to determine if the correct strips had been hit. As a result of this, the uncertainty of the strip # is not negligible. It should also be noted, that the source was placed directly in front of strip #8 and thus not

in the center of the setup.

When the simulations had been made, the mean energy of each simulation was plotted as a function of the front strip number. It is important to note, that the mean energy could be affected by the tail in the energy distribution but we expect the tail to have approximately the same effect on each of the simulations. The results of this are shown in figure 3.4.

The uncertainties has been calculated using standard deviation of the mean [5], $error = \frac{\sigma}{\sqrt{n}}$, where n is the number of detected particles. As a result of a large number of simulated particles, the errors of the mean energies are smaller than the points in the figure. Furthermore, the uncertainties in the strip numbers are expected to be of more importance. Taking these uncertainties into account, the angular effect is clear, and thus particles traversing the detector at larger angles do deposit a larger amount of energy. It should be noted, that the effect is on the keV scale and is thus not a prominent effect especially not in the thin detectors.

It is also clear that the effect does not seem to be symmetric around the center of the detector. This does though make sense as the source was placed in front of strip #8 - and thus we would also expect the effect to be symmetric around strip #8 as seen at the figure.

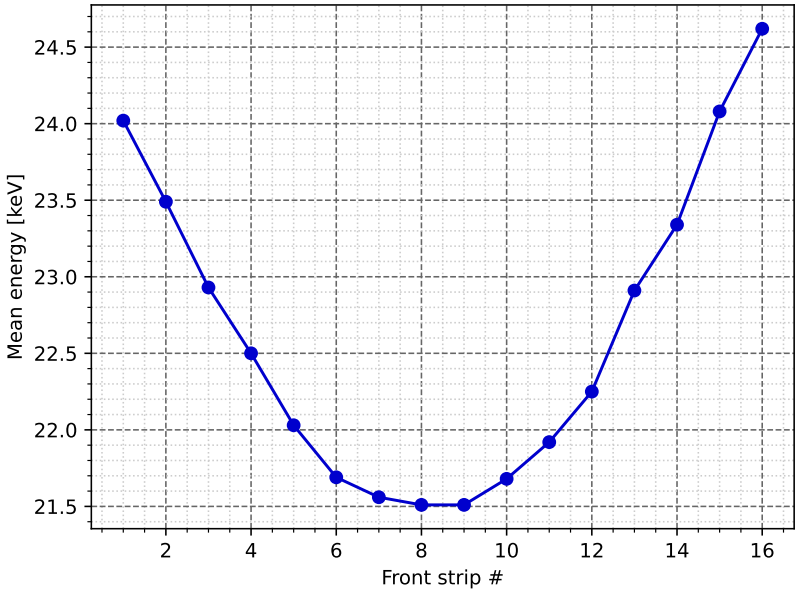

Figure 3.4: *The figure shows the result of 16 individual simulations where a monoenergetic source of electrons has been pointed towards each of the 16 front strips of a thin W1 detector. For each of the simulations, the mean energy deposited by the electrons has been plotted as a function of the front strip number. A thorough description of the figure and the uncertainties is found in the text.*

3.1.4 Backscattering in the setup

In real experiments, backscattered particles cannot be distinguished from non-backscattered particles. It is thus of interest to study how the effects of backscattering can be seen in the setup. To study this, a simulation with 10 million 5 MeV monoenergetic electrons and only the detectors present was used. Here, the particle source was aimed at the center of front strip #8 of W1-3, and the particles detected in the other detectors are therefore characterized as backscattered particles.

The distribution of the particles along the front strips of each W1 detector can be seen in figure 3.5 and the distribution along the back strips can be found in the appendix in figure A.1. When looking at the distribution along the front strips, it is clear that only a fraction of the number of particles detected in W1-3 is detected in the other 5 detectors. It thus therefore be noted, that it is only a fraction of the particles that are backscattered.

Furthermore, it is also worth noting how the backscattered particles are distributed along the front strips. When looking at the subfigures of figure 3.5, it is very clear that the angular effect discussed in section 3.1.3 is also present. A larger amount of backscattered particles are seen at the strips closest to W1-3 compared to those strips furthest away from W1-3. It should here be noted, that all of the detectors do not have the bottom part turning in the same direction. As an example, W1-2 and W1-4 (the detectors to the right and to the left of W1-3 seen from the center of the cube) are both facing with front strip #1 toward W1-3 as one detector is turned upside down compared to the other one. A description of the placement of the detectors can be found in figure 3.5.

When looking at the distribution along the back strips, we do not see the same effects. This is expected as the back strips are orthogonal to the front strips and hence we only see the angular effect as seen in figure 3.3.

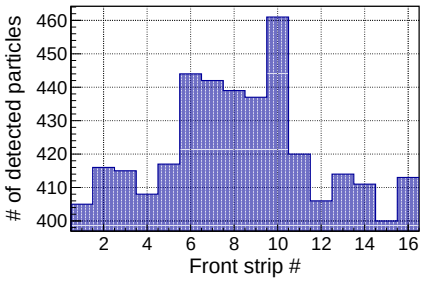

(a) *W1-1, placed directly across from W1-3. Front strip #1 is across from front strip #16 of W1-3.*

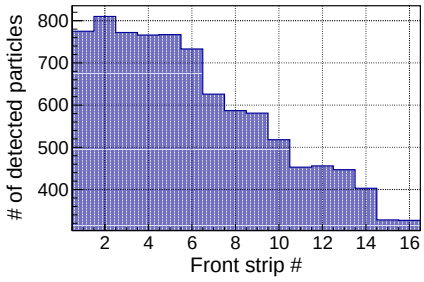

(b) *W1-2, placed to the right of W1-3 seen from the inside of the cube. Front strip #1 is facing towards W1-3.*

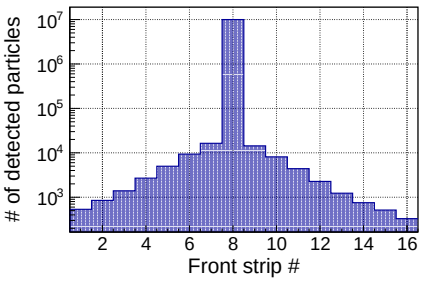

(c) *W1-3, the electrons are shot directly at the middle of front strip #8. Note the logarithmic scale at the y-axis.*

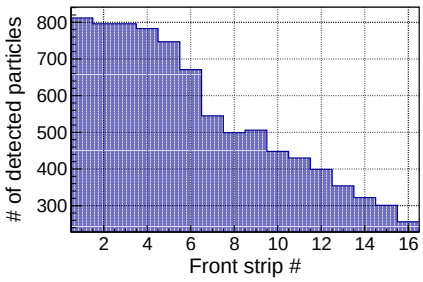

(d) *W1-4, placed to the left of W1-3 seen from the inside of the cube. Front strip #1 is facing towards W1-3.*

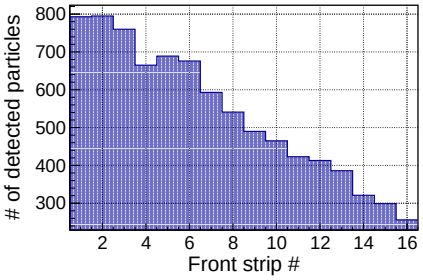

(e) *W1-5, the top of the cube when W1-3 is facing with the wires downwards. Front strip #1 is facing towards W1-3.*

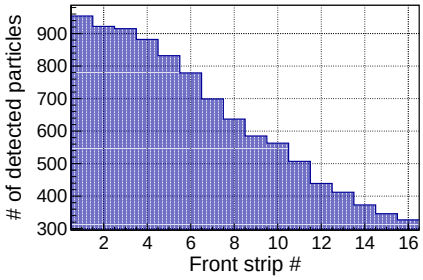

(f) *W1-6, the bottom of the cube when W1-3 is facing with the wires downwards. Front strip #1 is facing towards W1-3.*

Figure 3.5: *A simulation with 10 million* 5 MeV *monoenergetic electrons and only the detectors present was used to depict the results of backscattering in the setup. The electron source was aimed at front strip #8 of W1-3 and the particles detected in the other detectors are therefore characterized as backscattered particles. For each of the W1 detectors, the number of detected particles is shown as a function of the front strip number. A further description of the effects can be found in the text. In figure A.1, the distribution along the back strips can be seen.*

3.1.5 Solid angle coverage

To calculate the solid angle coverage of the detectors, a large simulation with 10 million particles, isotropic angular distribution, and only with the detectors present was used. The simulation was done with α particles as they do not backscatter as much as β particles. If β particles had been used instead, too many particles would be measured as some of the particles would be measured twice due to backscattering and this would result in a too-large solid angle coverage.

However, as α particles were used, it is only possible to measure the solid angle coverage of the W1 detectors as the α particles are stopped in these and they are not detected in the pad detectors. One should be aware that the pads are further apart compared to the W1s and the active area is not the same as for the W1s. As a result, the solid angle coverage would expectedly be smaller for the pads than for the W1s.

To calculate the solid angle coverage of the W1 detectors, the number of detected particles for each detector has been found. This gives us a total of 54.33(2)% detected particles which is assumed to be a close approximation to the solid angle of the W1 detectors. The number of detected particles used to calculate the solid angle coverage can be found in table 3.1.

Detector	**1**	**2**	**3**	**4**	**5**	**6**	**Sum**
Count	883,623	897,779	885,139	885,577	931,642	949,056	$5,432,816(2,331)$

Table 3.1: *The number of detected particles of each W1 detector in the setup when using a 10 million α particle source with uniform angular distribution is given. Note, that the uncertainties on the count is approximated as $\sqrt{count}$. The law of error propagation has been used to calculate the uncertainty on the sum.*

3.2 Monoenergetic β^- sources

After testing the simulations by checking that they reproduced known physical effects, the backscattering of β particles was studied further. At first, simple monoenergetic sources were used to eliminate effects from the energy spectra of realistic sources.

3.2.1 Backscattering as a function of energy

The backscattering is expected to depend on the initial energy of the β particles and to study this, the fraction of backscattered particles has been plotted as a function of the initial energy of monoenergetic electrons. To check how big an

effect the pad behind the W1 has on the backscattering, this was done both with and without the pad in telescope 3.

For this purpose, several simulations with 1 million electrons and only the detectors present were made. Again, a source pointing towards front strip #8 of telescope 3 was used and the fraction of backscattered particles was determined. The results of these simulations can be seen in figure 3.6. The uncertainties have been calculated using error propagation but as the number of simulated particles does not have any uncertainty, the uncertainties were calculated to be of the order of $10^{-4} - 10^{-5}$ and they are thus contained in the points.

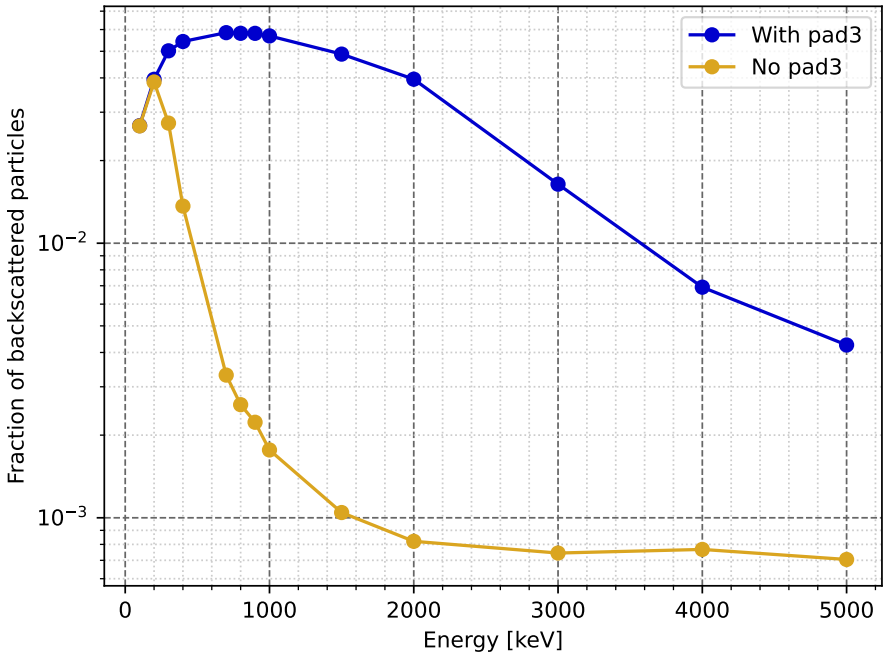

Figure 3.6: *The fraction of backscattered particles is shown as a function of the initial energy of the electrons for the two situations where only W1-3 of telescope 3 is present and with the complete telescope present. To do this, several simulations with 1 million electrons only with the detectors present with the source pointing towards front strip #8 of telescope 3 were made. The uncertainties are contained in the points and a more detailed description of the figure can be found in the text.*

The difference between the situation with the complete telescope 3 present and only with W1-3 present can be boiled down to a change in the thickness of the material that the particles can backscatter in — we would thus expect these two situations to scale linearly. But looking at figure 3.6, we can indeed see, that this is not the case. If we look at it roughly only taking the thickness of the active layers into account, the ratio of the thicknesses of the two situations can be calculated as $\frac{1497\,\mu\text{m}+65\,\mu\text{m}}{65\,\mu\text{m}} = 24$. We see that at smaller energies below 1 MeV, the ratio is lower than 24. Then between 1 MeV and 3 MeV, the ratio

is higher than 24 and again at 3 MeV and above, the ratio is again lower than 24. The reason for the fraction being smaller at lower energies is probably due to the particles being stopped and absorbed in the detectors, so even if the particles are scattered at an angle allowing for backscattering, many of these low-energy particles will not escape the detector again before they are stopped.

This shows us, that there is no linear scaling between the two situations and thus we will need to make simulations with a realistic setup and source to be able to understand a specific situation.

3.2.2 Backscattering as a function of detector thickness

We just saw in section 3.2.1 that there did not seem to be a linear scaling between the two situations as expected. This motivates us to look at backscattering as a function of the thickness of the detectors for different energies.

To do this, we look at a situation where we change the thickness of the active layer of a pad without any back dead layer. Here, thickness 0 refers to the original thickness of the active layer which is 1497 µm for pad-3 that has been used for this. A thickness smaller than 0 then refers to the active layer being thinner than the original size and a thickness larger than 0 will then naturally refer to a pad with an active layer thicker than the original size.

To study this, simulations with 1 million monoenergetic electrons pointing towards telescope 3 where only the detectors were present have been used. The fraction of backscattered particles has been plotted as a function of the thickness of the active layer of pad-3 for 1, 5, and 10 MeV and the results can be seen in figure 3.7. The uncertainties have again been calculated using error propagation and as they are of the order of 10^{-4} - 10^{-5}, they are thus also contained in the points.

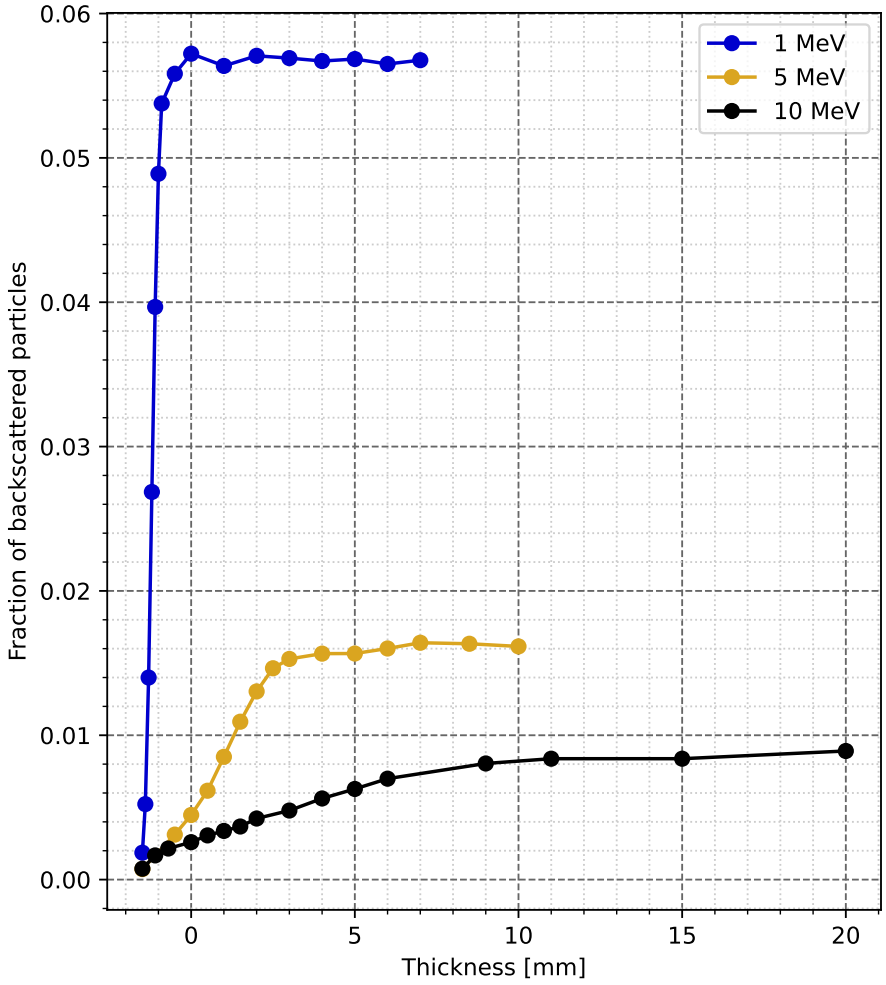

Figure 3.7: *The fraction of backscattered particles is plotted as a function of the thickness of pad-3 for three different energies. Note, that thickness 0 refers to the original thickness of the active layer, which is* 1497 µm *for pad-3 that has been used for this. A thickness smaller than 0 refers to the active layer being thinner than the original size and a thickness larger than 0 naturally refers to a pad with an active layer thicker than the original size. A description of the figure can be found in the text.*

Looking at figure 3.7, we clearly see that the fraction of backscattered particles clearly depends on the energy of the electrons as we also saw in figure 3.6. However, it is also clear, that the fraction of backscattered particles saturates at different thicknesses for different energies. Especially for small energies, the fraction of backscattered particles reaches saturation around the thickness of pad-3 and we will thus not see a linear correlation between the thin and the thick detectors for smaller energies. For larger energies, we do see a linear tendency for a larger range of thicknesses but these do eventually also saturate.

This means, that if the detectors are changed in a setup, new simulations will most likely be needed to describe the backscattering in the setup as the fraction of backscattered particles does not scale linearly for all changes in the thickness of the detectors at all energies.

3.2.3 Backscattering in the setup

All of the previous simulations have looked at backscattering in a setup with only the detectors present. From now on, we look at three different situations; first when only the detectors are present, then when both the detectors and their frames are present, and last where both the detectors, the frames, and the cube is present.

At first, we look at how large a fraction of the simulated particles is detected as a function of the energy of the electrons in the three situations. To study this, several simulations with 1 million monoenergetic electrons and isotropic angular distribution have been made and the results can be seen in figure 3.8. In section 3.1.5, the solid angle coverage of the W1 detectors was found to be 54.33(2)% and thus we must assume that if we detect a larger fraction of the simulated particles, this must be due to backscattering in the setup.

The uncertainties have been calculated using error propagation and as the errors are of the order of 10^{-4}, the errors are contained in the points. The figure clearly shows us, that the fraction of backscattered particles clearly depends on the energy of the electrons and the amount of backscattered particles peaks at around 1250 keV. Furthermore, it can be seen, that the presence of the frames and the cube has a clear effect on the fraction of backscattered particles. This effect is only prominent for energies larger than 100 keV and only the cube makes a difference at energies above 4 MeV.

However, it should also be noted that for all of the simulated energies in the situation with only the detectors present, more particles are detected than the measured solid angle coverage allows for. This shows us, that the detectors themselves contribute a noticeably amount to the backscattering. At 1250 keV, where the fraction of backscattered particles peaks, the detectors actually detect 64.5% of the simulated particles. This corresponds to roughly 10 percentage points more than what the solid angle coverage allows for.

It should thus be expected, that the effect of backscattering is largest for sources with smaller β energies and the main contributor to the backscattering is the detectors themselves even though the other parts of the setup also contribute to the backscattering.

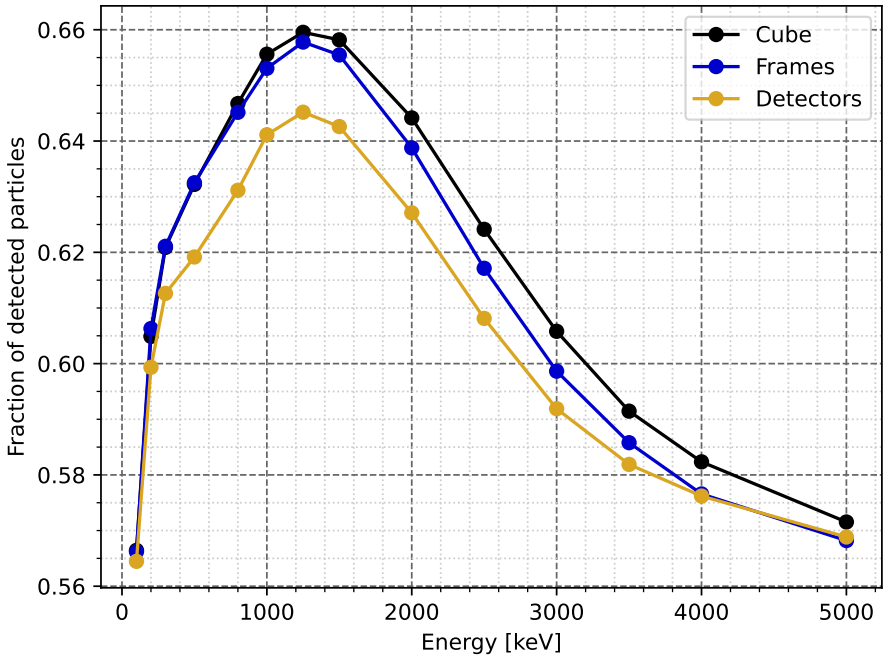

Figure 3.8: *The fraction of the simulated particles that are detected is plotted as a function of the energy of the simulated electrons for a source of 1 million electrons with an isotropic angular distribution. This is plotted for three situations; only with the detectors present, with both the detectors and their frames present, and with both the detectors, their frames, and the cube present. The errors are contained in the points. A more detailed description of the characteristics can be found in the text.*

3.2.4 Deposited energy using different setups

As we saw in section 3.2.3, adding the frames and the cube increases the number of backscattered particles. In the real experiment, there is a threshold of around 250 keV and it is thus interesting to study how the increase in the fraction of backscattered particles changes the distribution of the deposited energy of the electrons.

To examine this, simulation with 10 million monoenergetic 2 MeV electrons with isotropic angular distribution were used. The number of detected particles was then plotted as a function of the deposited energy of the electrons. This was completed for the same three situations as in section 3.2.3 and the results can be seen in figure 3.9.

The figure clearly shows that mainly two effects are present. The first effect is a clear increase of electrons at energies below 400 keV both in the situation where the frames are added to the setup but also in the case where the cube is also

added to the setup. The other effect shows a larger amount of detected particles at larger energies. Here, the amount of detected particles is especially increased when the cube is added to the setup. The increase of detected particles at lower energies is not as worrying as the threshold in the real experiment will eliminate the main part of this effect. The larger number of detected particles at larger energies is however more worrying as one would not be able to distinguish the electrons that have not been backscattered from those that have. It should also be noted that the clear cutoff at 2 MeV obviously is due to the electron energy being 2 MeV.

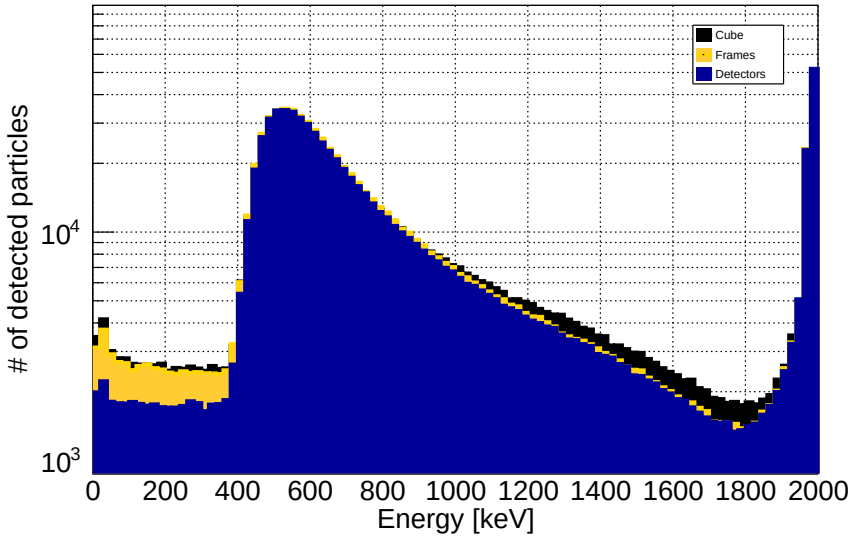

Figure 3.9: *The graph shows the number of detected particles as a function of the deposited energy of the electrons for the response of Pad-4. This is shown for three situations. The first situation is where only the detectors are present, in the second situation the frames have also been added, and in the last situation both the detectors, the frames, and the cube is present. A more detailed description of the characteristics is found in the text.*

3.2.5 Angular distribution of backscattered particles

We can see that the backscattering due to the frames and the cube changed the energy distribution of the detected particles noticeably both at low energies but also at higher energies. Thus, it is also interesting to see whether the backscattering in the setup also changes the angular distribution of the β particles in the setup.

To do this, the simulations described in section 3.2.3 have been used to plot the number of detected particles as a function of the front strip number of detector W1-6. Furthermore, we also saw that the detectors themselves did

contribute noticeably to the backscattering. Thus, it is also interesting to compare the results of these simulations with the ideal case where no β particles are backscattered. As β particles do backscatter, we are not able to make such a simulation with β particles, but as we are only looking at the angular distribution of the particles, a simulation with α particles could act as the ideal situation. The simulation with α particles used in section 3.1.5 is thus used again as the perfect scenario where no β particles are backscattered.

The result of these simulations can be seen in figure 3.10. It is very clear, that the number of detected particles is increased for each added element but it is harder to tell whether the angular distribution has been changed noticeably even though it could seem so.

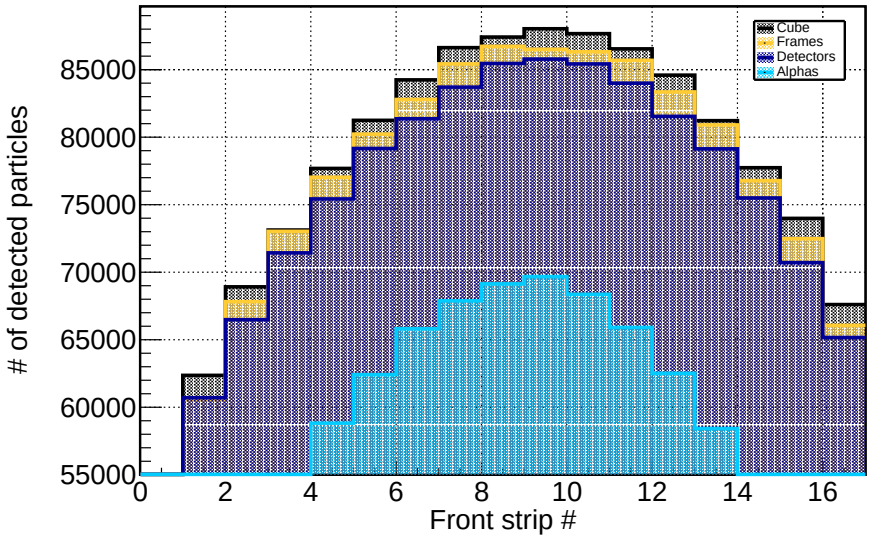

Figure 3.10: *The number of backscattered particles is shown as a function of the front strip number for the front strips of detector W1-6. This is depicted for the four situations; the ideal situation with no backscattering of the electrons, only with the detectors present, with the detector and the frames present, and at last with both the detectors, their frames, and the cube present. A more detailed discussion of the tendencies can be found in the text.*

To study this further, each bin in the histogram representing the situation with the cube present has been divided by the individual bins in the histogram representing the situation only with the detectors present. Furthermore the same has been done for the situation with the cube present and for the ideal situation. The errors of the data have been calculated using error propagation. If the two histograms follow the same distribution, we would expect their ratio to be close to constant however if they follow different distributions, we would expect to see a tendency in their ratio. The results can be seen in figure 3.11.

Looking at figure 3.11a, there does not seem to be a clear tendency - only maybe at the higher strip numbers where the ratio tends to be a bit higher. If we instead look at figure 3.11b, it is very clear that that the two histograms do not follow the same distribution. From this, we can thus see that the effect of the detectors, the frames, and the cube altogether does change the angular distribution of the backscattered particles of a monoenergetic source of 2 MeV.

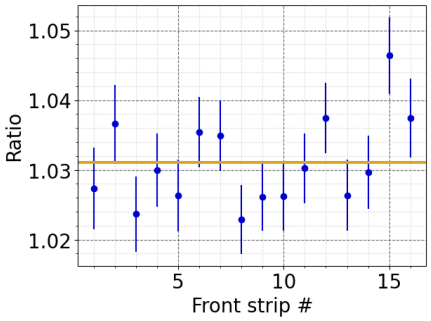

(a) *The ratio of the two histograms from figure 3.10 showing the angular distribution of the particles with only the detectors present and with the detectors, their frames, and the cube present. The orange bar shows the average value of the points.*

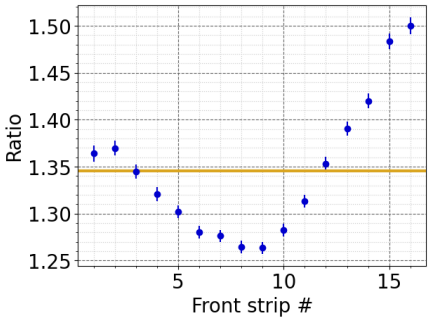

(b) *The ratio of the two histograms from figure 3.10 showing the angular distribution of the ideal situation (simulated with α particles) and with the detectors, their frames, and the cube present. The orange bar shows the average value of the points.*

Figure 3.11: *The two subfigures show two different ratios of histograms for detector W1-6. From these, one can see that the distributions two distribution compared in figure (b) does not follow the same distribution. A more detailed description can be found in the text.*

3.3 Realistic β^- sources

In the previous sections, all of the simulations have been made using monoenergetic sources and starting from this section, more realistic sources was used. For the main parts of this section, a ^{12}B source with a realistic energy distribution and isotropic angular distribution was used. Furthermore, the carbon foil and the frame of the source have been added to make the source more realistic. This also means that we no longer deal with a point source, but instead, the source is a plane circle with a radius of 0.45 cm.

3.3.1 Backscattering in the setup

Using a realistic ^{12}B source, three long (10 million) simulations have been made for the same three situations as discussed in section 3.2.3. The number of detected particles for each W1 detector has been noted and the increase in the number of detected particles has been calculated which can be seen in table 3.2.

Here, we see that the number of detected particles increases by 0.48(59)% when both the frames and the cube is added compared to the situation where only the detectors are present. However, in section 3.2.5, we did see that the largest increase in backscattered particles actually came from the detectors themselves and not from the frames and the cubes. If we instead compare the number of detected particles with the ideal situation using an α source as before, we see a much larger effect. In the case with only the detectors present, we see 1.0734(6) times as many particles as in the ideal situation where no particles are backscattered. If both the frames and cube are also present, we see 1.0786(6) times as many particles. The simulation described in section 3.1.5 has been used for these calculations as the ideal situation.

This means, that both the detectors, the frames, and the cube together give us 7.86(6)% more particles due to backscattering when using the realistic ^{12}B source. The backscattering is thus a very relevant effect that should be taken into account when performing experiments.

Det #	Detectors	Frames	Cube	Cube/Detectors
1	935,804	935,704	938,798	1.0032(15)
2	1,045,055	1,048,949	1,050,442	1.0052(14)
3	936,560	937,989	936,990	1.0005(15)
4	936,109	935,239	937,711	1.0017(15)
5	929,429	928,814	936,583	1.0077(15)
6	1,048,856	1,047,728	1,059,330	1.0100(14)
Sum	$5,831,813(2,415)$	$5,834,423(2,415)$	$5,859,854(2,421)$	
Fraction	1	1.00045(59)	1.0048(6)	

Table 3.2: *The number of detected particles are given for three different situations. On all of the counts, the uncertainties are given by $\sqrt{n}$ with n being the number of counts. The uncertainties of the sums and fractions has been calculated using the law of error propagation.*

3.3.2 Deposited energy using different setups

We saw in section 3.2.4 that the backscattered particles due to the frames and the cube changed the energy distribution of the detected particles for a monoenergetic 2 MeV source. It is thus of interest to check how prominent this effect is for the realistic ^{12}B source. Using the same three simulations with β particles as in section 3.3.1, the same plot has been made for pad-4 which is seen in figure 3.12.

Here, we see that the effects are clearly smaller. Especially the effect at larger energies are definitely not as prominent as for the monoenergetic 2 MeV source however, the effect at the low energies is still present. This decrease in the effects is not surprising as the fraction of backscattered particles is higher for lower energies, and as the energy of the monoenergetic 2 MeV source is much smaller than the energy of the realistic ^{12}B source, this was expected.

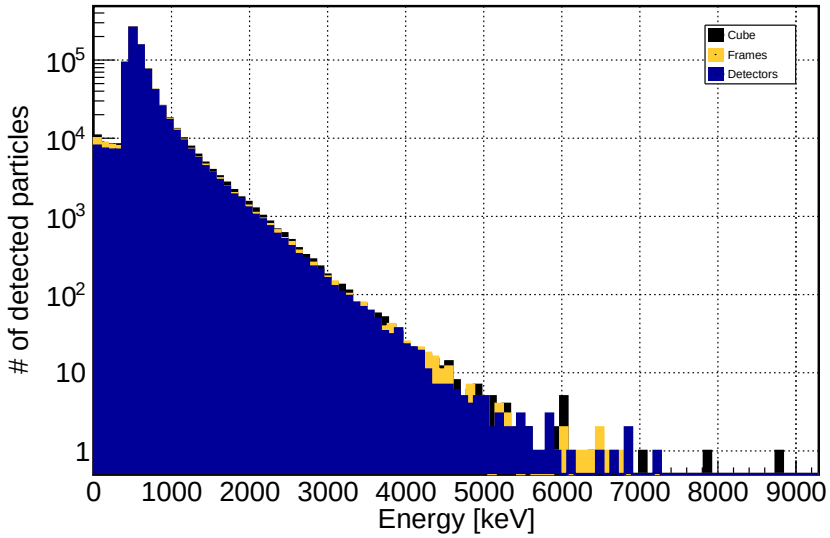

Figure 3.12: *The graph shows the number of detected particles as a function of the deposited energy of the electrons for the response of pad-4. This is shown for three situations. The first situation is where only the detectors are present, in the second situation, the frames have also been added, and in the last situation both the detectors, the frames, and the cube is present. A more detailed description of the characteristics is found in the text.*

3.3.3 Angular distribution of backscattered particles

We now want to make the same analysis as in section 3.1.3 but with the realistic ^{12}B source instead. This has been completed both without a threshold and with a threshold of 250 keV. In the following sections, we will go through the analysis for both of these situations.

Realistic ^{12}B source without a threshold

Using the same simulations as in section 3.3.1 together with the same simulation with α particles as in section 3.2.5, the same plot as in figure 3.10 has been made for the realistic ^{12}B source. This plot can be seen in figure 3.13.

Here, we see that the number of detected particles increases noticeably again when adding more elements to the setup but it is again hard to tell with the naked eye if the added elements change the angular distribution along the strips. To examine this further, the same plots as in figure 3.11 have been made for the new realistic source and the results are depicted in figure 3.13.

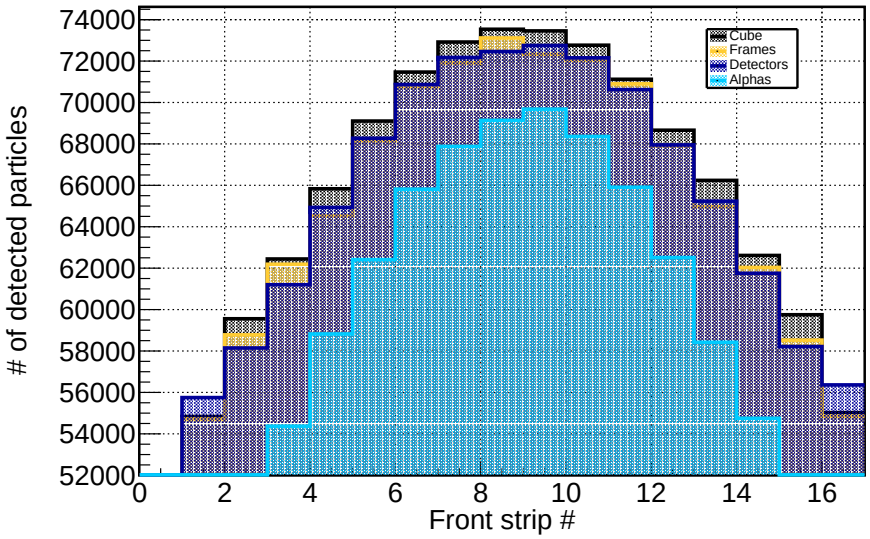

Figure 3.13: *The number of backscattered particles is shown as a function of the front strip number for the front strip of detector W1-6. This is depicted for the four situations; the ideal situation with no backscattering of the electrons, only with the detectors present, with the detector, and the frames present, and at last with both the detectors, their frames, and the cube present. In this situation, the simulations did not include a threshold. A more detailed discussion of the tendencies can be found in the text.*

Looking at figure 3.14b it is clear, that the angular distribution of the β particles is not the same for the case of the ideal case with no backscattering as for the case where both the detectors, the frames and the cube contribute to backscattering. When looking at the figure, we see a variation in the ratio of more than 15% - it is thus very clear that the distribution of the particles has been changed considerably by the setup itself. It should also be noted that the backscattered particles mainly increase the amount of particles close to the edges of the detector.

If we instead look at figure 3.14a, we actually also see a tendency but the variations are not as large as when comparing with the ideal case. This means, that adding the frames and the cube to the setup also changes the angular distribution of the particles compared to the case where only the detectors are present. However, this effect is not as prominent. As a result, it will be necessary to make new simulations if the setup changes to ensure the effect of backscattering in the setup has not changed.

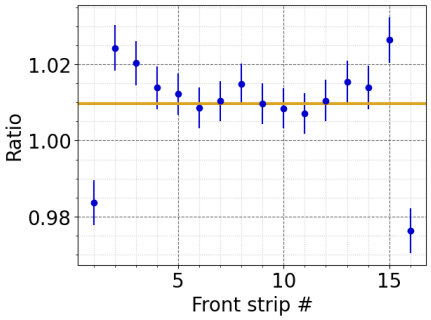

(a) The ratio of the two histograms from figure 3.13 showing the angular distribution of the particles with only the detectors present and with the detectors, their frames, and the cube present. The orange bar shows the average value of the points.

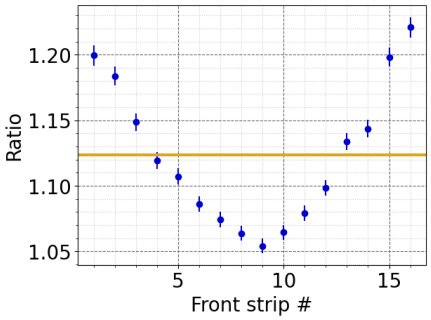

(b) The ratio of the two histograms from figure 3.13 showing the angular distribution of the ideal situation (simulated with α particles) and with the detectors, their frames, and the cube present. The orange bar shows the average value of the points.

Figure 3.14: *The two subfigures show two different ratios of histograms for detector W1-6. Both of the figures are comparisons with simulations without thresholds. A detailed description can be found in the text.*

Realistic ^{12}B source with a threshold of 250 keV

The real experiment has a threshold due to the electronics of the system. It is thus of interest to study how this threshold can affect the angular distribution of the particles. To study this, identical simulations for β particles as used in section 3.3.3 have been made - only with a threshold of 250 keV. Furthermore, the same figures as in section 3.3.3 has also been produced. Note, that the simulation with the α particles is still the same and this simulation does not include any threshold. As the source does not have the same energy distribution as the realistic ^{12}B source, using a threshold would be misleading. Because of this, the number of detected particles for the ideal case will be larger compared to the other simulations but we can still compare the angular distributions.

The angular distributions along the front strips are depicted in figure 3.15. Again, the tendencies are harder to study by looking at this figure, and thus figures 3.16a and 3.16b gives us a more clear view of this again.

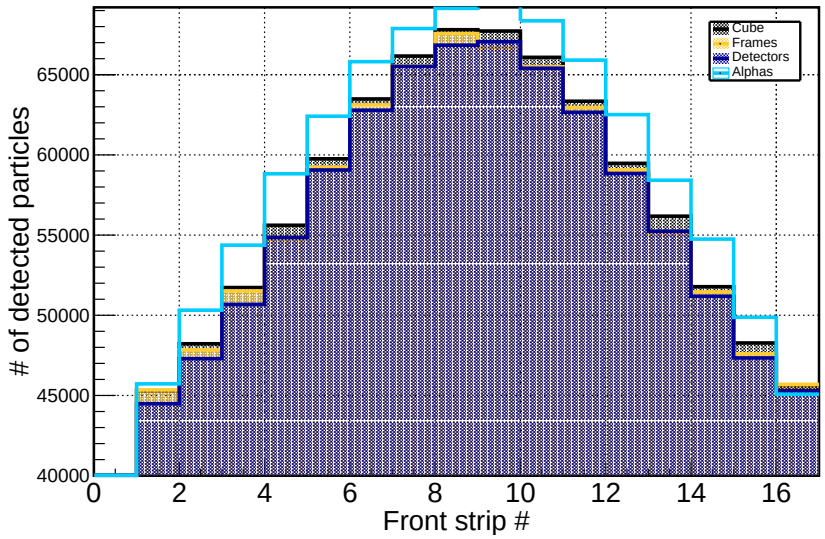

Figure 3.15: *The number of backscattered particles is shown as a function of the front strip number for the front strip of detector W1-6. This is depicted for the four situations; the ideal situation with no backscattering of the electrons, with only the detectors present, with the detector, and the frames present, and at last with both the detectors, their frames, and the cube present. In this situation, the simulations included a threshold of* 250 keV*. A more detailed discussion of the tendencies can be found in the text.*

Looking at figure 3.16a, a small tendency can be seen indicating that the angular distributions of the situation with only the detectors present and with both the detectors, the frames, and the cube present are not exactly the same. This indicates, that adding the frames and the cube to the setup can change the angular distribution of the β particles even though a threshold is present. However, this effect is still not as prominent an effect as the effect of the detectors themselves.

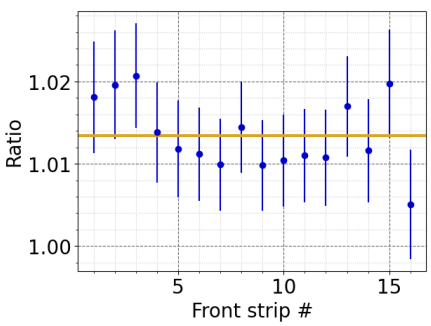

(a) The ratio of the two histograms from figure 3.15 showing the angular distribution of the particles with only the detectors present and with the detectors, their frames, and the cube present. The orange bar shows the average value of the points.

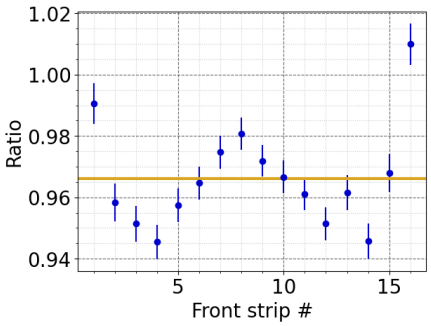

(b) The ratio of the two histograms from figure 3.15 showing the angular distribution of the ideal situation (simulated with α particles) and with the detectors, their frames, and the cube present. The orange bar shows the average value of the points.

Figure 3.16: *The two subfigures show two different ratios of histograms for detector W1-6. Both of the figures are comparisons with simulations with β particles with a threshold of* 250 keV*. However, it should be noted, that the simulation with α particles does not include a threshold. A detailed description can be found in the text.*

If we instead take a look at figure 3.16b, we clearly see that the two angular distributions are not the same for the ideal case and for the case with the cube and the other elements present. However, it should be noted that when comparing this situation with figure 3.14b, where no threshold was present, the ratio of the angular distributions has also changed considerably. In the case with no threshold, we saw one minimum almost in the middle of the detector. But in the case with a threshold, we have a local maximum in the middle of the detector and two minima instead. It is thus clear, that a threshold can also change the angular distribution of the particles. This must thus indicate that particles of the same energies are not detected uniformly in the strips of the detectors.

To examine this more precisely, the ratio between the two histograms showing the number of detected particles with and without a threshold for the situation with both the detectors, the frames, and the cube present has been produced and can be seen in figure 3.17. Here it is clear that the two situations do not follow the same distribution. Adding the threshold seems to mostly remove particles from the front strips closest to the edges of the detector. It should also be noted, that the variation along the strips is quite large and thus this is a quite large effect.

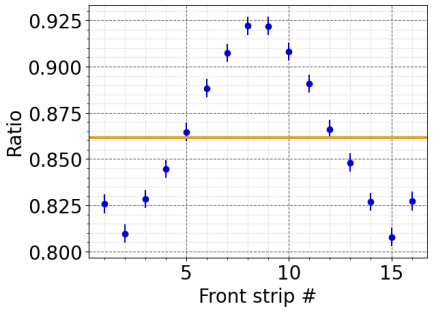

Figure 3.17: *The ratio of the two histograms for detector W1-6 showing the number of detected particles for the situation with both the detectors, the frames, and the cube present with and without a threshold of* 250 keV*. More specifically, the ratio is given by the bins of the histogram with the threshold divided by the bins histogram without the threshold. In the text, a further discussion of the results can be found.*

3.3.4 Helium

We saw in figure 3.6 that the fraction of backscattered particles depends heavily on the energy of the electrons. To check the effect of backscattering for a source with lower energy, two simulations with a ${}^{6}_{2}\mathrm{He}$ source was made; one only with the detectors present and one with all of the former simulated elements in the setup. This showed, that there were $6,322,700 \pm 2,500$ detected particles when only the detectors were present and $6,471,500 \pm 2,500$ detected particles when both the frames and the cube were present. This means, that there were detected 1.0235 ± 0.0006 times more particles with the frames and the cube present compared to the case where only the detectors were present.

If we, again, compare with the ideal case simulated in section 3.1.5, this shows us that there were detected 1.1912(7) times as many particles as the ideal case where no β particles are scattered in the setup. Backscattering is thus a very prominent effect for sources with lower energies.

Conclusions

In this thesis, Geant4 was used to study the the β^- response of two different detectors; a simple silicon pad detector and the W1 detector which is a double sided silicon strip detector. Furthermore, the framework has been used to study the effects of backscattering in a complex setup which has been used for experiments at IGISOL.

A main part of this thesis has been to further development the program, G4Sim, which has been used to study the β^- response and the effects of backscattering. Using the framework, Geant4, turned out to be a good choice as the program has solved the posed problems. Using Geant4 for almost half a year, some quirks have however presented themselves and a further description of some of these can be found in chapter 2.

The simulations and results obtained using G4Sim can mainly be divided into three categories; testing the program, simulations with monoenergetic sources, and simulations with realistic sources.

Making simulations to test the program has been an important aspect of making G4Sim as we should be able to rely on the program working correctly. The results of these tests showed that G4Sim reproduced realistic energy spectra of deposited energy both with β^- and α particles and for both of the simulated detectors. Furthermore, the program reproduced two angular effects of a point source with an isotropic angular distribution. The first effect causes fewer particles be detected in the outermost strips of the W1 detectors and the second effect instead causes the particles traversing the detector at larger angles to deposit more energy in the detectors. Furthermore, the simulations could also produce backscattering with a realistic angular distribution when only shooting particles towards the center of one detector. Finally, the solid angle coverage of the W1 detectors of the setup was calculated to be 54.32(2)% using α particles as they do not backscatter noticeably in the setup.

After G4Sim had been tested thoroughly, simulations with monoenergetic β^- sources became the main focus. Here we saw that the fraction of backscattered particles depends on the energy of the incident electrons and that the backscattering is highest for lower energies peaking at 1250 keV. Furthermore, we saw

that for lower energies, there is no linear dependency between the fraction of backscattered particles for a thin and a thick detector. However, at higher energies we did see a linear correlation which saturated at different thicknesses for different energies. For 5 MeV particles, the saturation started at detectors thicker than 3 mm and for 10 MeV particles, the saturation instead started at detectors thicker than 6 mm. This means, that the linear dependency only holds for large energies and thin detectors.

Furthermore, we also saw that the fraction of backscattered particles depends on the elements present in the setup. It is clear, that the detectors themselves pose the largest cause of backscattering but both the frames and the cube also causes a measurably increased fraction of backscattered particles. We saw that for 1250 keV particles, the detectors, the frames, and the cube increased the fraction of detected particles with more than 10 percentage points compared to what the solid angle allows for.

Using a monoenergetic 2 MeV source, it was also clear that the energy distribution of the deposited energy was changed when the frames and the cube was added to the setup. A larger amount of particles were detected at energies below 400 keV primarily due to the frames and a larger amount of particles were detected at higher energies primarily due to the cube.

Looking at the angular distribution of the β^- particles, we also saw that especially the backscattered particles due to the detectors themselves, did change the angular distribution noticeably for the monoenergetic sources.

In the experiment at IGISOL, a ^{12}B source was used. Thus to be able to make simulations comparable with the real experiments, a realistic ^{12}B source was created. Using this source, we saw that with only the detectors present 1.0734(6) times as many particles were detected compared to what the solid angle allows for. Adding the frames and the cube to the setup increased the fraction to 1.0786(6). This means, that the detectors, the frames, and the cube altogether results in 7.86(6)% more particles being detected due to backscattering when using a realistic ^{12}B source - and the detectors are the main contributors.

Looking at the energy distribution, we did not see as large a change using the realistic source however, a larger amount of particles below 400 keV was still detected. Instead looking at the angular distribution of the particles, it was clear that the presence of both the detectors, the frames and the cube did change the angular distribution of the particles noticeably as more particles were detected primarily at the edges of the W1 detector. Furthermore, we also saw that when comparing the situation only with the detectors present to the situation with all of the elements present, the angular distribution was also changed - however, this effect was not as prominent.

In the real experiment, the electronics of the system causes a threshold and thus it has also been studied what the effect of the threshold could be on the angular distribution of the β^- particles. Here we saw that the angular distribution of the particles still changed both when comparing the situation with all of the elements present with the ideal case with no backscattering in the setup and

with the situation with only the detectors present. Again, the effect of the latter was still not as prominent as the former.

Comparing the two situations with and without the threshold, it was also clear that adding the threshold did change the angular distribution of the particles considerably. Here it was clear that adding the threshold primarily removed particles detected at the edges of the side of the detector.

At last, a simulation with ^{6}He was made to study the effect of backscattering for a source with a lower energy. Here we clearly saw that the effect of backscattering was enhanced. With both the detectors, the frames, and the cube present, 1.1912(7) times as many particles were detected compared to the ideal case with no backscattering in the setup. Thus, this is a prominent effect especially for sources with lower energies.

Concluding, this means that backscattering of β^- particles does increase the amount of detected particles considerably in the setup used at IGISOL and the backscattering does change the angular distribution of the detected β particles in this setup. The main contributor to the backscattering and to the changes in the angular distributions was the detectors themselves and thus we would also expect to see the same effects in the experiment performed with the ^{12}N source.

This means, that in general backscattering must be taken into account when doing experiments with β^- particles. The backscattering and the angular distribution of the particles depend on the setup and thus new simulations must be performed when changes to the setup or to the source are made. We also saw that this is especially important for sources with lower energies and when the thicknesses of the detectors are changed even though the setup otherwise stays the same.

For future prospects it could be of interest to study the angular distributions of ^{6}He to see how the large fraction of backscattered particles affects the angular distribution of the β particles. Furthermore, it could also be interesting to study the angular effects of all of the 6 W1 detectors in the setup at IGISOL to see if the changes to the angular distribution is the same for all of the detectors or if it differs.

Improvements could also be made to G4Sim by adding the tube that the cube was placed in thereby making it possible to examine the effects this might have on the backscattering in the setup. Furthermore, the time frame of this project was limited to 5 months and hence the program itself could also be improved. More specifically it could be of interest to make it possible to add and remove the frames and the cube in the macro such that the setup could be changed after compilation. At last, the measurements of the cube and the frames are currently also hard-coded into the program but it would be better if these values were read from a JSON file instead, just as it is the case for the detectors.

References

[1] Dennis Wright (SLAC) and Sebastien Incerti (CNRS/IN2P3). *PHYSICS OVERVIEW AND PROCESSES*. Slideshow. URL: http://geant4.in2p3.fr/IMG/pdf_Physics2.pdf (visited on 05/09/2021).

[2] 2003 IEEE Nuclear Science Symposium - Medical Imaging Conference. *Basic structure of Basic structure of the Geant4 Simulation Toolkit*. Lecture notes. 2003. URL: https://www.ge.infn.it/geant4/training/portland/basicStructure.pdf (visited on 09/05/2021).

[3] Andreas Gad. "From Helium to Carbon and Oxygen". Progress report of Ph.d. Department of Physics and Astronomy, Aarhus University, Apr. 2020.

[4] Aarhus University Subatomic physics group. *AUSAlib*. https://git.kern.phys.au.dk/ausa/ausalib/wikis/home. Apr. 2021.

[5] Ifan Hughes and Thomas Hase. *Measurements and their uncertainties: a practical guide to modern error analysis*. Oxford University Press, 2010.

[6] F Knoll Glenn. "Radiation detection and measurement". In: *General Properties of Radiation Detectors* (2000).

[7] NIST. *ASTAR : Stopping Power and Range Tables for Alpha Particles*. URL: https://physics.nist.gov/cgi-bin/Star/ap_table.pl (visited on 06/08/2020).

[8] NIST. *ESTAR : Stopping Power and Range Tables for Electrons*. URL: https://physics.nist.gov/cgi-bin/Star/e_table.pl (visited on 06/08/2020).

[9] nuclear-power.net. *Silicon – Atomic Number – Atomic Mass – Density of Silicon*. 2019. URL: https://www.nuclear-power.net/silicon-atomic-number-mass-density/ (visited on 06/08/2020).

[10] Bogdan Povh et al. *Particles and nuclei*. Springer, 1995.

[11] S Tanuma, Cedric J Powell, and David R Penn. "Calculations of stopping powers of 100 eV–30 keV electrons in 31 elemental solids". In: *Journal of Applied Physics* 103.6 (2008), p. 063707.

[12] Tostevin.net. *Photo Voltic Cells (Solar Panels)*. URL: http://tostevin.net/?p=2241 (visited on 06/04/2020).

[13] The Nuclear Data group at the Triangle Universities Nuclear Laboratory (TUNL). *Energy Level Diagrams A=12*. 2018. URL: `https://nucldata.tunl.duke.edu/nucldata/figures/12figs/menu12.shtml` (visited on 02/06/2021).

[14] S Viñals et al. "Calibration and response function of a compact silicon-detector set-up for charged-particle spectroscopy using GEANT4". In: *The European Physical Journal A* 57.2 (2021), pp. 1–9.

Appendix A

Appendix

A.1 Installation guide to G4Sim

To install G4Sim with working visualization, the following things should be installed in the order below:

- Root
- AUSALib
- Sorter
- Calibrator
- Geant4
- G4Sim

In the following, we will use a structure with a folder, named tools, where all of the relevant things are installed. This folder is simply placed in the `/home/username` folder, so you should start by making this folder. Also note, that in the following, when the folder "sheila" is used (this is my username), you should change it to your own username.

A.1.1 Root

To install root, you should follow the guide at this CERNs oficial website[1]. First make sure, that you have the required dependencies - you can also check this at CERNs official website [2].

[1] `https://root.cern/install/`
[2] `https://root.cern/install/dependencies/`

When you have installed the required dependencies, you should "cd" into the tools folder and run the following commands, which has been copied from the website:

```
wget https://root.cern/download/root_v6.22.00.Linux-ubuntu19-x86_64-gcc9.2.tar.gz
tar -xzvf root_v6.22.00.Linux-ubuntu19-x86_64-gcc9.2.tar.gz
source root/bin/thisroot.sh # also available: thisroot.{csh,fish,bat}
```

Then update your `.bashrc` file - this can for example be done by using vim (`vim ~/.bashrc`) with the following line (make sure to change your username):

```
source /home/sheila/tools/root/bin/thisroot.sh
```

You should then check if the installation has worked by typing `root` in the same and a new terminal.

A.1.2 AUSALib

To install AUSALIB, you should again "cd" into the tools folder and run the following commands.

```
cd ~/tools
git clone https://gitlab.au.dk/ausa/ausalib.git
cd ausalib
mkdir build
cd build
cmake ..
make -j8
```

You should now add the following lines to your `.bahrc` file again.

```
export AUSALIBPATH="home/sheila/tools/ausalib"
export AUSALIB_INC_DIR="$AUSALIBPATH/include"
export AUSALIB_LIB_DIR=$"AUSALIBPATH/build"
```

A.1.3 Sorter

The sorter should be installed in a very similar way using the running the following commands.

```
cd ~/tools
git clone https://gitlab.au.dk/ausa/sorter.git
cd sorter
mkdir build
cd build
cmake ..
make -j8
```

You can then check if it works by typing the following command.

```
~/tools/sorter/build/Sorter --help
```

A.1.4 Calibrator

The installation of the calibrator is identical to the sorter - and you should thus run the following commands.

```
cd ~/tools
git clone https://gitlab.au.dk/ausa/calibrator.git
cd calibrator
mkdir build
cd build
cmake ..
make -j8
```

You can then check if it works by typing the following command.

```
~/tools/calibrator/build/Calibrator --help
```

A.1.5 Geant4

Installing GEANT4 is the tricky part. At first, you should make sure you have all of the required dependencies. You can do this by running these commands:

```
sudo apt install qtbase5-dev libgl1-mesa-dev libx11-dev \
libxmu-dev libmotif-dev libxerces-c-dev
```

Afterwards, you should create a folder called "geant4_build" in the tools folder. Then do the following (it will take around 20-60 minutes depending on your computer).

```
git clone https://gitlab.cern.ch/geant4/geant4.git
cd geant4
mkdir build
cd build
cmake -DCMAKE\_INSTALL\_PREFIX=/home/sheila/tools/geant4\
    _build -DGEANT4\_INSTALL\_DATA=ON -DCMAKE\_BUILD\_TYPE=
    Release -DGEANT4\_USE\_GDML=ON -DGEANT4\_USE\_OPENGL\
    _X11=ON -DGEANT4\_USE\_XM=ON -DGEANT4\_USE\_QT=ON -
    DGEANT4\_BUILD\_MULTITHREADED=ON ../
make install
```

After this, you should add a lot of lines to your `.bashrc` file - you can find the updated list at the official website for Geant4[3]. Make sure to check that the folders do not have updated names or versions. For me, this means, that I added the following lines to my file.

```
source /home/sheila/tools/geant4_build/bin/geant4.sh

export Geant4_LIB_DIR=/home/sheila/tools/geant4build
export Geant4_DIR=/home/sheila/tools/geant4Build
export G4ABLADATA="/home/sheila/tools/geant4/build/data/
    G4ABLA3.1"
export G4ENDFSTATEDATA="/home/sheila/tools/geant4/build/data
    /G4ENDFSTATE2.3"
export G4INCLDATA="/home/sheila/tools/geant4/build/data/
    G4INCL1.0"
export G4LEDATA="/home/sheila/tools/geant4/build/data/
    G4EMLOW7.13"
export G4LEVELGAMMADATA="/home/sheila/tools/geant4/build/
    data/PhotonEvaporation5.7"
export G4NEUTRONHPDATA="/home/sheila/tools/geant4/build/data
    /G4NDL4.6"
export G4PARTICLEXSDATA="/home/sheila/tools/geant4/build/
    data/G4PARTICLEXS3.1.1"
export G4PIIDATA="/home/sheila/tools/geant4/build/data/
    G4PII1.3"
export G4RADIOACTIVEDATA="/home/sheila/tools/geant4/build/
    data/RadioactiveDecay5.6"
export REALSURFACEDATA="/home/sheila/tools/geant4/build/data
    /RealSurface2.2"
export G4SAIDDXSDATA="/home/sheila/tools/geant4/build/data/
    G4SAIDDATA2.0"
```

[3] https://geant4-userdoc.web.cern.ch/UsersGuides/InstallationGuide/html/postinstall.html#environment-variables-for-datasets

You should now have a working installation of GEANT4. Check this by running exampleB1 and make sure that visualization works.

```
cd geant4/examples/basic/B1
mkdir build
cd build
cmake ..
make
./exampleB1
```

A.1.6 G4Sim

G4Sim can be installed using the guide at github[4] guide.

At first, remember to make sure that you have installed boost. If not, install it by running the following commands.

```
sudo apt install libboost-all-dev
```

Then install G4Sim.

```
git clone https://gitlab.au.dk/au479664/G4Sim.git
cd G4sim
mkdir build
cd build
cmake ..
make -j8
```

You can now check, that everything works by running the following line from the build folder in G4Sim.

```
./main ../res/macros/vis.mac
```

You can also test it with other macro files, if you like.

[4] https://gitlab.au.dk/au479664/G4Sim/-/wikis/Installation**this**

A.2 Figures

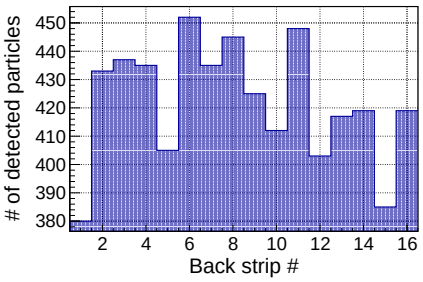

(a) W1-1, placed directly across from W1-3. Back strip #1 placed at the top as for W1-3.

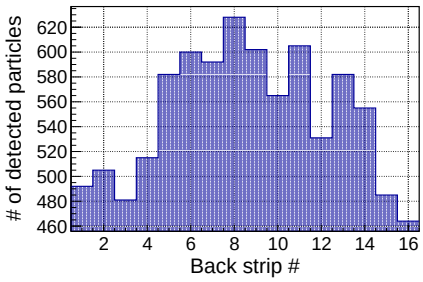

(b) W1-2, placed to the right of W1-3 seen from the inside of the cube. Back strip #1 placed at the top as for W1-3.

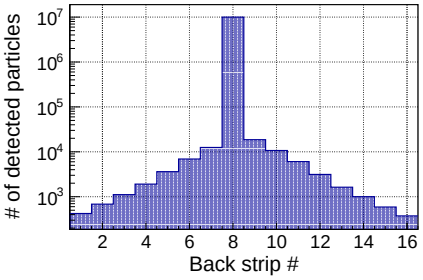

(c) W1-3, the electrons are shot directly at the middle of back strip #8. Note the logarithmic scale at the y-axis.

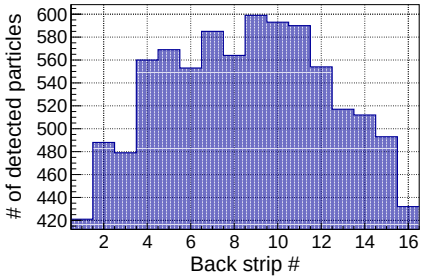

(d) W1-4, placed to the left of W1-3 seen from the inside of the cube. Back strip #1 placed at the bottom (opposite of W1-3).

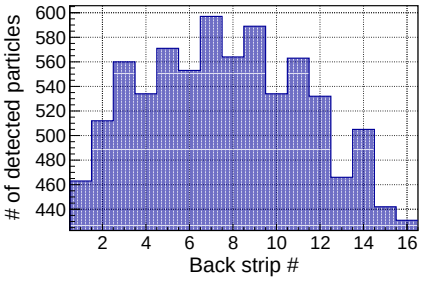

(e) W1-5, the top of the cube when W1-3 is facing with the wires downwards. Back strip #1 is facing towards front strip #1 of W1-3.

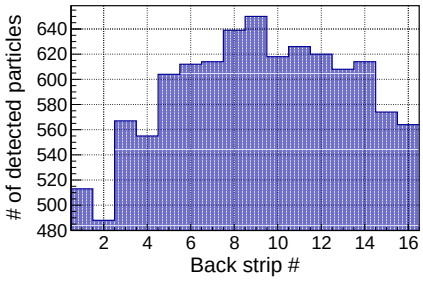

(f) W1-6, the bottom of the cube when W1-3 is facing with the wires downwards. Back strip #1 is facing towards front strip #16 of W1-3.

Figure A.1: *A simulation with 10 million* 5 MeV *monoenergetic electrons and only the detectors present was used to depict the results of back scattering in the setup.The electron source was aimed at the center of detector 3 and the particles detected in the other detectors are therefore characterized as back scattered particles. For each of the W1 detectors, the number of detected particles are shown as a function of the back strip number. In figure 3.5, the distribution along the back strips can be seen.*